A GPVI-platelet-neutrophil-NET axis drives systemic sclerosis

Roxane Darbousset[1], Leetah Senkpeil[1,2], Julia Kuehn[1], Spoorthi Balu[1], Dhruv Miglani[1], Eilish Dillon[3], Caroline Fromson[4], Mehreen Elahee[3], Pierre-Andre Jarrot[5], Sydney B. Montesi[4], Deepak A. Rao[3], Jerry Ware[6], Denisa D. Wagner[5], Andreea M. Bujor[7], Maria Gutierrez-Arcelus[1,2], Peter A. Nigrovic[1,3,*]

Affiliations
[1]Division of Immunology, Boston Children's Hospital, Harvard Medical School, Boston, MA, USA. [2]Broad Institute of MIT and Harvard, Cambridge, MA, USA. [3]Division of Rheumatology, Inflammation, and Immunity, Brigham and Women's Hospital, Harvard Medical School, Boston, MA, USA. [4]Division of Pulmonary and Critical Care Medicine, Massachusetts General Hospital Boston, Massachusetts. [5]Program in Cellular and Molecular Medicine, Boston Children's Hospital, Harvard Medical School, Boston, MA, USA. [6]Department of Physiology and Cell Biology, University of Arkansas for Medical Sciences, Little Rock, AR, USA. [7]Arthritis and Autoimmune Diseases Center, Department of Medicine, Boston University Chobanian and Avedisian School of Medicine, Boston, MA, USA.

***Corresponding author:** peter.nigrovic@childrens.harvard.edu

Author contributions: R.D. and P.A.N. designed the study. R.D., J.K., and S.B., D.M. performed animal experiments. R.D. performed *in vitro* experiments, R.D. and J.K. performed histology and imaging analysis. L.S. and M.G.A. analyzed transcriptomic data, E.D., C.F., M.E., P.A.J., S.B.M, D.R., J.W., D.D.W., M.B. provided technical or material support and consultation. R.D. and P.A.N. wrote the manuscript.

Competing interests: D.D.W. reports research support from Pliant Therapeutics and Boehringer Ingelheim, consulting for Accendatech USA, APIE Therapeutics, DevPro Biopharma, Mediar Therapeutics, Neutrolis, Pliant Therapeutics, and Roche, and speaking fees from Cowen. P.A.J. reports research support from SOBI, Roche, and GSK. P.A.N. reports research support from BMS and Pfizer, consulting for Alkermes, Apollo, Century Therapeutics, Cerecor, Exo Therapeutics, Merck, Monte Rosa, Novartis, and Pfizer, and equity in Edelweiss Immune, Inc. None of these conflicts are related to the work presented.

Data and materials availability: All data associated with this study and not present in the current manuscript can be available upon reasonable request.

ABSTRACT

Systemic sclerosis (SSc) is characterized by progressive fibrosis of skin, lung, and other organs and retains among the highest rates of mortality among autoimmune diseases. We identified activation of circulating neutrophils from patients with diffuse SSc, together with concordant transcriptomic evidence of neutrophil activation in blood, skin, and lungs, and in mice with experimental SSc of skin and lung induced by hypochlorous acid or bleomycin. Neutrophil depletion abrogated experimental SSc, while adoptive transfer of SSc neutrophils induced skin and lung fibrosis in healthy mice, identifying neutrophils as both necessary and sufficient for disease. In patients, platelet activation accompanied diffuse SSc, and in mice platelet activation preceded neutrophil activation, suggesting an upstream role. Platelet depletion abrogated both neutrophil activation and tissue fibrosis. SSc platelets conferred upon neutrophils the capacity to induce SSc. This capacity corresponded to enhanced production of neutrophil extracellular traps (NETs); experimental SSc was abrogated in NET-deficient PAD4$^{-/-}$ mice, a resistance bypassed by adoptive transfer of PAD4-suficient SSc neutrophils, confirming NETs as a key effector mechanism of SSc. In turn, platelet activation was mediated via the platelet collagen receptor GPVI, while GPVI deficiency resulted in attenuated platelet and neutrophil activation, fewer circulating NETs, and protection from fibrosis in both murine models of SSc. Together, these findings define a GPVI-platelet-neutrophil-NET axis in SSc and identify a new set of therapeutic targets in this often-refractory condition.

INTRODUCTION

Systemic sclerosis (SSc), also known as scleroderma, is a chronic autoimmune disease characterized by vascular abnormalities, immune system dysregulation, and widespread fibrosis with excess deposition of extracellular matrix components including collagen (*1-3*). Fibrosis affects the skin, but can also involve the lungs, gastrointestinal tract, and heart, especially in diffuse SSc (dSSc), the most aggressive form of the disease, leading to considerable morbidity and mortality (*3-5*).

Beyond fibrosis, SSc features a substantial inflammatory component (*1, 6*). Chronic inflammation can precede and accompany the fibrotic process (*6-9*). The presence of neutrophils correlates with a poor prognosis in bronchoalveolar (BAL) fluid and other tissues (*10-12*). Yet evidence for neutrophil activation in SSc has varied between studies, and their role as *in vivo* pathogenic effectors remains to be established (*13-17*).

Endothelial injury occurs early in SSc, potentially as the primary lesion, a possibility suggested by clinical and histological studies and by the observation that environmental agents linked to SSc-like syndromes are generally also endothelial toxins (*18, 19*). Multiple mechanisms connect vascular injury to tissue fibrosis, including immune cell activation, hypoxia, thrombosis, and endothelial-to-mesenchymal transition (*20, 21*). In this context, platelets are of interest. Platelets from SSc patients exhibit evidence of activation, with enhanced expression of surface markers such as P-selectin (*22-24*). Some authors have identified unusual susceptibility of SSc platelets to activation by collagen, a protein exposed when the endothelial lining is disrupted (*18, 25-28*). Patients with SSc exhibit an abundance of circulating platelet-derived microparticles capable of activating neutrophils and potentially other cells, and adoptive transfer of these microparticles mediates endothelial injury in lung (*16, 29*). However, how platelets become activated and whether platelets and neutrophils play essential roles *in vivo* remains to be established.

Here we studied circulating neutrophils and platelets in patients with dSSc and tested the contribution of neutrophils, neutrophil extracellular traps (NETs), and platelets to fibrosis in murine models of SSc that exhibit neutrophil and platelet phenotypes comparable to those observed in human dSSc. We establish that both neutrophils and platelets play essential roles in SSc pathogenesis, in a cascade initiated through the platelet collagen receptor glycoprotein VI (GPVI) and ending with platelet-induced NET formation, thereby identifying a new set of potential therapeutic targets in this challenging disease.

RESULTS

Neutrophils are activated in diffuse systemic sclerosis

We began by characterizing neutrophils from the peripheral blood of patients with dSSc, compared with healthy controls (Supplemental Table 1 for demographic and phenotypic information). In dSSc patients, the proportion of neutrophils among all leukocytes and the absolute abundance of these cells in circulation were both increased, as was the neutrophil-to-lymphocyte ratio (Figure 1 A-C). Circulating neutrophils expressed more total and active-conformation Mac-1 integrin and a trend to less L-selectin (Supplementary Figure 1 A for gating strategy; Figure 1 D-F). Neutrophils from dSSc patients also exhibited greater ROS production in the absence of additional stimulation, as well as enhanced migration toward chemoattractant in a transwell system (Figure 1 G, H, Supplemental Figure 1 B for representative flow cytometry plots). Correspondingly, biopsy tissue from lesional skin revealed an increase in neutrophils in patients compared to controls (Supplemental Figure 1C). Thus, neutrophils are both abundant and exhibit an activated phenotype in dSSc.

To test the generalizability of these findings, we aggregated 8 publicly available transcriptomic datasets comparing dSSc patient samples with controls for lung biopsy tissue (40 dSSc, 24 controls), skin biopsy tissue (219 SSc, 112 controls), and whole blood (111 dSSc, 80 controls) (Supplemental Figure 2 A & B). Considering all samples together, differential gene expression analysis revealed 85 up-regulated genes and 16 downregulated genes in dSSc using fold-change cutoff of 0.5 and a Benjamini-Hochberg FDR corrected p value of 0.05 (Figure 1 I). Gene set enrichment analysis (GSEA) ranked by based on all fold-changes (2201 genes up, 1180 down) identified a signal for neutrophil degranulation (normalized enrichment score (NES) 2.07, $p=7.0\times10^{-5}$ corrected for multiple comparisons), alongside expected pathways such as interferon signaling and extracellular matrix biology (Figure 1 J). We then examined organ specificity. Differential gene expression analysis revealed 285, 2068, and 585 up-regulated genes in the lung, skin and blood, respectively, of dSSc patients compared to controls (Supplemental Figure 3 A-C). GSEA identified neutrophil degranulation as enriched in affected lung (NES 2.67, corrected $p=1.5\times10^{-4}$) and skin (NES 1.87, corrected $p=8.5\times10^{-5}$), though this signal was depleted in blood (NES -2.93, corrected $p=2.3\times10^{-10}$) (Supplemental Figure 3 A-C). Normalizing for batch effects using data from healthy controls (see Methods), we compared lung vs. blood from dSSc patients, finding neutrophil degranulation as the most enriched pathway in lung (NES 3.30, corrected $p=1.73\times10^{-20}$); comparing skin vs. blood, neutrophil degranulation was the second most enriched pathway (NES 2.55, corrected $p=1.06\times10^{-17}$) (Supplemental

Figure 3 D & E). Together with our flow cytometry and histology data, these findings establish neutrophils as a population of interest in dSSc, justifying further exploration of their functional contribution.

Murine models of SSc feature neutrophil activation resembling human dSSc

SSc-like fibrosis of skin and lung can be induced in wild-type C57Bl/6 mice by repeated intradermal injection of the ROS donor hypochlorous acid (HOCl-SSc) or by subcutaneous injection of the chemotherapeutic agent bleomycin (BLM-SSc) (*30, 31*). We evaluated the profibrotic role of neutrophils in these two systems, comparing SSc mice to controls receiving injections of PBS (Supplemental Figure 4 A & B for model design). Only female animals were employed since male mice developed skin necrosis and could not be studied humanely (not shown).

At harvest, day 42 in HOCl-SSc and day 28 in BLM-SSc, SSc mice exhibited increased dermal thickness (Figure 2 A). Lung fibrosis also developed, as quantified by a modified Ashcroft histological score (*32*) and by lung collagen content (Figure 2 B & C). HOCl-SSc and BLM-SSc animals developed increased serum anti-Scl-70 autoantibody levels, as previously reported in both models as well as in human dSSc (*33-35*) (Figure 2 D). In both models, circulating neutrophils displayed changes comparable to those we had observed in human patients, including higher surface Mac-1, lower surface L-selectin, greater ROS production, and enhanced migration toward chemoattractant (Figure 2 E-J, Supplemental Figure 4 C & D). In BAL fluid, we observed a fourfold increase in neutrophils in BLM-treated mice compared to controls, although not in the slower-acting HOCl-SSc model (Supplemental Figure 4 E & F); however, both models exhibited a clear increase in neutrophils in perfused and disaggregated lung tissues, as a percentage of all cells and by absolute count (Supplemental Figure 4 G-J). These results support HOCl-SSc and BLM-SSc as appropriate models to study the pathogenic relevance of neutrophils in dSSc.

Neutrophils mediate fibrosis in murine SSc

To test the role of neutrophils in the development and progression of fibrosis in SSc, we depleted neutrophils by administration of 100 μg of anti-Ly6G antibody (clone 1A8) vs. irrelevant isotype control (clone 2A3) daily for 7 days then every 48 hours. Starting from day 7, mice received HOCl or BLM to induce SSc (Supplemental Figure 5 A). Neutrophil depletion (~80%) was sustained for up to 49 days, markedly attenuating dermal thickness and lung fibrosis in both

models (Figure 3 A-H, Supplemental Figure 5 B).

To test whether neutrophils directly mediate fibrosis, we employed adoptive transfer. Neutrophils were isolated by negative selection from bone marrow of mice treated with PBS (day 28 or 42), HOCl (day 42), or BLM (day 28); 5×10^6 cells were then injected either into heathy recipients (Supplemental Figure 5 C & D). Cells were injected either intradermally (i.d) for the effect on skin or intravenously (i.v) for the effect on lungs. After 2 weeks, mice were euthanized to assess skin and lung tissues. Remarkably, neutrophils from SSc mice induced fibrosis in the skin and lungs of healthy mice, whereas those from PBS-treated animals did not (Figure 3 I-N). As a methodological control, we transferred isolated T cells from PBS- or HOCl-treated mice; these cells failed to induce fibrosis (Supplemental Figure 5 F-I). Together, these findings identify neutrophils as both necessary and sufficient for induction of experimental SSc.

Neutrophils release NETs to mediate fibrosis in SSc

Next, we sought to determine how neutrophils mediate tissue fibrosis. Among neutrophil effector functions, formation of NETs is particularly interesting. NETs promote inflammation through mechanisms including induction of pro-inflammatory cytokines and chemokines (*36, 37*), activation of immune cells (*38, 39*), and generation of oxidative stress (*40, 41*). NETs also induce epithelial-mesenchymal transition (*42-44*), activate fibroblasts (*45, 46*), and facilitate extracellular matrix deposition (*47, 48*). Human patients with SSc exhibit elevated circulating NET remnants (*14, 29*). We observed that dSSc neutrophils stimulated with the calcium ionophore A23187 released more NETs than those from control donors, as assessed by basal CitH3 release. Interestingly, dSSc but not healthy neutrophils spontaneously generated NETs during culture (Figure 4 A, Supplemental Figure 6 A). We therefore explored whether neutrophils contribute to SSc via NETs.

In both HOCl-SSc and BLM-SSc mice, neutrophils exhibited enhanced spontaneous NET release, although unlike human dSSc no difference was observed after stimulation with the calcium ionophore A23187 (Figure 4 B & C). NET formation is contingent upon chromatin decondensation (*49*), mediated through histone H1, H3 and H4 deimination by peptidyl arginine deiminase 4 (PAD4), an enzyme highly expressed in neutrophils (*50*). In all conditions, CitH3 was essentially absent in neutrophils from $PAD4^{-/-}$ animals, confirming the specificity of the assay for NETosis (Figure 4 B & C).

In vivo, mice subjected to HOCl and BLM treatment exhibited a notable increase in NETosis, as assessed by the levels of CitH3 in both serum and lung tissue (Figure 4 D and Supplemental Figure 6 A, B). PAD4$^{-/-}$ mice exhibited markedly reduced fibrosis in skin and lung in both HOCl-SSc and BLM-SSc, with levels of CitH3 reduced to control levels in lung homogenates (Figure 4 E-H and Supplemental Figures 6 B-F). Correspondingly, total collagen content in whole lung was reduced in PAD4$^{-/-}$ mice compared to WT mice (HOCl-SSc, Supplemental Figure 6 G). Adoptive transfer of neutrophils from SSc mice induced skin and lung fibrosis in healthy PAD4$^{-/-}$ recipients, confirming a specific role for neutrophil NETs as opposed to other effects of PAD4 deficiency (Figure 4 I-L). Interestingly, PAD4 deficiency did not reduce neutrophil activation as assessed by surface Mac-1 and L-selectin, although PAD4$^{-/-}$ mice did show reduced basal ROS production (Supplemental Figure 6 H-M). These data implicate NET formation as a critical endpoint of neutrophil activation contributing to fibrosis in SSc.

Platelets are activated during SSc and participate in fibrosis

We then sought to understand how neutrophils become activated during SSc. Our attention focused on platelets because of their established role in neutrophil activation and migration (*51-53*). Excess platelet activation was also identified by our GSEA analyses, overall as well as from sub-analyses of skin but not lung (overall NES 1.98, $p=2.45\times10^{-3}$; skin NES 1.81, $p=3.10\times10^{-3}$; Figure 1 J, Supplemental Figure 3 B). In fresh citrate-anticoagulated whole blood from patients with dSSc, platelets exhibited increased surface P-selectin and phosphatidyl serine compared with healthy controls (Figure 5 A & B). Comparable changes were observed in mice treated with HOCl or BLM, showing that activation of circulating platelet is a feature shared across human and murine SSc (Figure 5 C-F, Supplemental Figure 7 A-C for gating strategy).

To determine whether platelets play a causal role in SSc, we generated mice in which expression of the diphtheria toxin (DT) receptor is expressed selectively in megakaryocytes and their daughter platelets (PF4^{cre}-iDTR), allowing near-total platelet depletion by administration of DT (*54*). We administered DT daily for 7 days then every 72h into PF4^{Cre+}/DTR$^{fl/fl}$ mice and PF4^{Cre-}/DTR$^{fl/fl}$ littermate controls, initiating HOCl-SSc on day 7 (Supplemental Figure 7 D for experimental design). Platelet depletion (>99%) was sustained for up to 49 days (Supplemental Figure 7 E). At day 42 following HOCl injections, dermal thickness was markedly decreased in platelet-depleted PF4^{Cre+}/DTR$^{fl/fl}$ compared to littermate controls treated with DT (Figures 5 G & H). Similarly, lung fibrosis was markedly reduced in mice subjected to platelet depletion (Figures 5 I & J).

To further test the profibrotic role of platelets, we performed adoptive transfer. Platelets isolated from HOCl- or PBS-treated mice were injected (5×10^6 platelets) intradermally or intravenously into heathy recipient animals (Supplemental Figure 5 C). After 2 weeks, skin and lung tissues were collected for histopathological evaluation. The transfer of platelets from HOCl-treated mice induced increased dermal thickness and a trend to increased lung fibrosis compared to mice receiving platelets isolated from control PBS-treated mice (Figure 5 K-N). Collectively, these findings confirm participation of platelets in fibrosis from experimental SSc.

Platelets trigger the profibrotic function of neutrophils in SSc

To evaluate whether the effect of platelets could be mediated through neutrophils, we assessed the kinetics of platelet and neutrophil activation in the slower HOCl model. Blood was collected at days 0, 14, 28 and/or 42 following initiation of HOCl or PBS treatment. Platelet activation was assessed by surface P-selectin and phosphatidyl serine, while neutrophil activation was monitored by surface Mac-1 and L-selectin as well as intracellular ROS. We observed that platelet activation began between day 14-28, preceding neutrophil activation by at least 2 weeks (Figure 6 A-E). In $PF4^{Cre+/}DTR^{fl/fl}$ mice, platelet depletion reduced neutrophil activation, as reflected in decreased Mac-1 levels and increased L-selectin (Figures 6 F & G). These findings position platelet activation before, and so potentially contributory to, neutrophil activation.

To test whether platelets act directly on neutrophils to enable SSc, we assessed the ability of platelets from mice treated with PBS, HOCl, or BLM to induce NETs in healthy neutrophils (Figure 6 H). Neutrophils isolated from healthy mice were co-cultured with SSc or PBS control platelets (1 neutrophil: 50 platelets). Vehicle and A23187 were used as negative and positive control, respectively. Indeed, platelets from HOCl-SSc and BLM-SSc induced NET formation as measured by released CitH3 (Figure 6 H). This finding was recapitulated with human samples, demonstrating that platelets from dSSc donors trigger NET formation in healthy neutrophils more than platelets from healthy donors (Figure 6 I).

These findings suggest that platelet-activated neutrophils could potentially mediate disease *in vivo*. To confirm this possibility, we performed adoptive transfer experiments using healthy neutrophils pre-incubated with HOCl-SSc platelets and then washed to remove excess platelets. Indeed, compared with neutrophils incubated with control platelets, neutrophils exposed to SSc platelets increased dermal thickness and lung fibrosis in previously healthy mice (Figure 6 J-M).

Thus, activated SSc platelets engage neutrophils as profibrotic effector cells via mechanisms including NETs.

Feedback activation of platelets by neutrophils in SSc

Neutrophils can promote platelet activation (*55, 56*). Indeed, HOCl-SSc and BLM-SSc mice depleted of neutrophils by 1A8 exhibited reduced platelet activation compared to those treated with 2A3, as reflected in lower expression of P-selectin and phosphatidyl serine (Supplemental Figures 8 A-D). PAD4$^{-/-}$ mice treated with HOCl or BLM similarly exhibited reduced platelet activation compared with controls (Supplemental Figure 8 E-H), suggesting that feedback from neutrophils to platelets is mediated via NETs, though reduced platelet activation might also result from other processes, such as attenuated tissue injury.

The platelet-neutrophil axis of fibrosis in SSc is initiated via the GPVI receptor

Finally, we sought to determine how platelets become activated in SSc. Microvascular injury is an early disease feature, leading to exposure of collagen beneath the damaged endothelium (*57-59*). Some but not all authors have identified a specific enhanced reactivity of human SSc platelets to collagen (*26-28*). In our GSEA of SSc skin when compared to blood, the platelet-restricted collagen receptor glycoprotein VI (GPVI) pathway emerged as significantly enriched (NES 2.09, corrected p= 8.05×10^{-3}, Supplemental Figure 3 B). We isolated platelets from 3 dSSc patients and sex-matched healthy donors and tested reactivity to ADP (agonist for the P2Y1 and P2Y12 receptors), thrombin (agonist for the protease activation receptors), and convulxin (agonist for GPVI). We observed a trend toward increased reactivity to convulxin, though this effect was obscured by substantial donor-to-donor variation (Supplemental Figures 9 A & B). In HOCl-SSc mice, selective platelet reactivity to GPVI ligation emerged clearly (Supplemental Figures 9 C & D). We therefore sought to test the role of GPVI in SSc.

To this end, we subjected GPVI$^{-/-}$ and littermate control GPVI$^{+/+}$ mice to HOCl- and BLM-induced SSc. Flow cytometry confirmed GPVI deficiency in platelets of GPVI$^{-/-}$ mice (Supplemental Figure 9 E & F). GPVI$^{-/-}$ platelets exhibited reduced P-selectin and phosphatidyl serine expression (Figure 7 A-D), consistent with impaired platelet activation. We observed a concurrent reduction in neutrophil activation, with lower Mac-1 expression and higher L-selectin expression (Figure 7 E-H). Serum CitH3 levels were also lower, indicating reduced NET formation (Figure 7 I). Histopathological examination of skin and lung sections confirmed a protective effect against fibrosis in GPVI$^{-/-}$ mice in both HOCl and BLM models (Figure 7 J-Q).

Together, these findings identify GPVI as a driver of platelet activation, neutrophil activation, NET release, and tissue fibrosis in SSc.

DISCUSSION

This study identifies a GPVI-platelet-neutrophil-NET-fibrosis axis in SSc. Our findings suggest a model whereby exposed collagen, potentially from injured endothelium (*16, 29*), activates platelets via the GPVI receptor, and that these cells, in turn activate neutrophils to release profibrotic NETs (Figure 8). Activated neutrophils further activate platelets, potentially via NETs, creating a reciprocal activation loop that may further accelerate disease. Established mechanistically in two independent murine models that share important biologic features with human dSSc, these finding further corroborated both by studies in dSSC patients and by findings in large transcriptomic datasets. The results thereby establish a direct role of neutrophils in dSSc and identify a set of potential new targets in this often-refractory disease.

Our findings are concordant with observational and experimental data collected about the role of neutrophils and platelets in SSc over the past several decades. Multiple authors have noted evidence of neutrophil activation in SSc, though some results diverge from this conclusion, potentially reflecting a mixture of dSSc (as studied here) with limited SSc, which is generally less severe (*13-17*). Platelet activation in SSc is well documented (*16, 27-29*). Given the focus of SSc research on fibrosis, and the relative paucity of neutrophils in SSc skin biopsies, these observations have received limited attention, and it has remained unclear whether neutrophil and platelet phenotypes are epiphenomenal or pathogenically relevant.

The mechanisms by which platelets activate neutrophils and by which these cells mediate fibrosis are likely multiple and complex. Maugeri and colleagues showed that platelet microparticles from SSc patients, and from healthy platelets stimulated with collagen, contain the alarmin HMGB1. This molecule acts directly upon neutrophils to promote autophagy, persist longer in circulation, and release NETs. Correspondingly, healthy mice treated with these microparticles exhibited evidence of microvasculopathy in lungs (*29*). Our data are fully compatible with these findings, showing in two murine models that platelet activation precedes neutrophil activation and that depletion of either neutrophils or platelets attenuates disease severity. Platelets also activate neutrophils directly via P-selectin PSGL-1, among other mechanisms (*60*). Further, we establish that NETs are not only a marker of neutrophil activation

in SSc but play a direct pathogenic role, and that the collagen receptor GPVI provides a key activating signal for platelets. Other platelet effector functions may also be relevant, both for neutrophil activation and for fibrosis generally. For example, studies in the Tsk-1 mice and BLM-SSc model have identified a profibrotic role for platelet serotonin, an effect that presumably proceeds independent of neutrophils (*61*).

The observation that GPVI is central to platelet activation in SSc is particularly interesting. It has been reasonable to assume that endothelial damage is at least partially responsible for platelet activation, and we now support this assumption by showing that a platelet receptor for a component of exposed subendothelial matrix is indeed directly relevant for disease. Importantly, GPVI is therapeutically targetable in humans. Individuals genetically deficient in GPVI exhibit a mild bleeding defect and many are asymptomatic, suggesting that interrupting this pathway may be relatively safe (*62, 63*). Some patients with idiopathic thrombocytopenic purpura (*78, 79*) and systemic lupus erythematosus (*80*) exhibit autoantibodies against GPVI, resulting in a phenotype of mild bleeding tendency and lack of collagen-induced platelet aggregation. Correspondingly, antibodies blocking GPVI are already in clinical development and have demonstrated preliminary evidence of efficacy and safety for conditions including stroke and carotid stenosis (*64-66*). Our findings pave the way for trials of GPVI inhibition in SSc patients, especially since GPVI blockade is not immunosuppressive and therefore might be safely combined with conventional immunomodulatory and anti-fibrotic agents.

A limitation of our studies is that mechanistic investigations are conducted in murine models of SSc. No murine model perfectly mimics human disease, and so extrapolation of findings to human SSc must be undertaken with caution. However, it is reassuring that essentially all findings tested were fully concordant between two mechanistically distinct systems, HOCL-SSc and BLM-SSc, and that both models closely recapitulated the neutrophil and platelet phenotypes that we established first in humans. Our human transcriptomic findings were generated by comparison of datasets generated separately, using different cell preparation methods, such that residual batch effects are difficult to exclude. Therefore, these results should be interpreted with caution, although we are reassured by concordance with our experimental findings.

Crucially, our data demonstrated that mice deficient in PAD4, an enzyme critical for NET formation, were protected against fibrosis in both SSc models, aligning with prior research in

SSc and aging (*67, 68*). PAD4-mediated histone citrullination facilitates NET release (*69*), a process observed predominantly in neutrophils but potentially involving other cells such as macrophages(*70, 71*), which may also have a role in SSc-related fibrosis (*72, 73*). The PAD4-deficient mice used in our studies were global knockouts and results from these experiments alone do not implicate neutrophil NETs directly. To establish the connection, we showed *in vitro* experiments confirming enhanced NETs formation in in both human and murine SSc and used adoptive transfer methods to show that WT SSc neutrophils induced fibrosis in PAD4-deficient mice. These data confirm neutrophils as a crucial source of NET-induced fibrosis in SSc, although they do not exclude a role for extracellular traps from other sources, or of other effects of PAD4. Recently, PAD4 inhibitors have gained interest for treatment of cancer, rheumatoid arthritis, and COVID (*74-77*), and our findings now support the addition of SSc to this list.

In conclusion, our study delineates a GVPI-platelet-neutrophil-NETs-fibrosis axis in SSc, providing new insights into disease mechanisms and identifying potential new therapeutic targets. Future research will focus on refining these findings and translating them into clinical applications aimed at improving outcomes for SSc patients.

MATERIAL AND METHODS

Animals

C57BL/6J (Jax # 000664), B6.Cg-Padi4tm1.1Kmow/J (PAD4$^{-/-}$, JAX # 030315), C57BL/6-Tg(PF4-icre)Q3Rsko/J (PF4-Cre, JAX # 008535), and C57BL/6-Gt(ROSA)26Sortm1(HBEGF)Awai/J (iDTR, JAX # 007900) mice were purchased from The Jackson Laboratory. Gp6tm1Ware/J (GPVI$^{-/-}$) mice were provided by Professor Jerry Ware. PF4^{Cre}-iDTR mice were generated by crossing PF4-icre mice with iDTR mice. The offspring PF4^{Cre+}/DTR$^{fl/fl}$ and PF4^{Cre-}/DTR$^{fl/fl}$ were used as experimental or littermate control mice, respectively. GPVI$^{-/-}$ mice were bred with C57BL/6 to generate heterozygous GPVI$^{+/-}$ mice. The GPVI$^{+/-}$ mice were them used to generate experimental GPVI$^{-/-}$or GPVI$^{+/+}$ littermate control mice. Genotypes were confirmed using Transnetyx. Both males and females 6-10 weeks old were used for breeding and 6-8-week-old females were used for SSc. Mice were housed under specific pathogen-free conditions within ventilated cages with food and water ad libitum, under constant room temperature and with 12h day-night cycles, at Boston Children's Hospital. All the procedures were approved under the Institutional Animal Care and Use Committee and operated under the supervision of the department of Animal Resources at Children's Hospital.

HOCl-SSc model

HOCl-SSc was induced as previously described (*81*) with slight modification. Briefly, 150 µl of an HOCl solution was intradermally injected in 2 sites (300 µl in total) into the shaved backs of mice, using a 27-gauge insulin syringe 5-days a week for 6 weeks. Control mice received injections of 300 µl of sterile phosphate-buffered saline (PBS). Mice were randomly allocated to experimental and control groups. HOCl was prepared fresh daily by adding NaClO solution (9-14% as active chlorine) to a 100 mM KH_2PO_4 solution (pH 6.2). The stock NaClO solution was kept no more than 6 weeks after opening. The NaClO concentration was determined at 292nm using a nanodrop (NanoDrop™ One, Thermo Fisher Scientific) and adjusted between OD 0.7 and 0.9.

Bleomycin-SSc model

BLM-SSc was induced as previously described (*31*). A sterile solution of 1mg/mL of bleomycin (Cayman chemicals) was in PBS. Bleomycin 100 µl was subcutaneously injected into the shaved backs of mice daily for 4 weeks using a 27-gauge insulin syringe. Control mice received injections of 100 µl of sterile PBS. Mice were randomly allocated into experimental and control groups.

Tissue collection and histopathologic analysis

Human skin biopsies were collected from the forearm of consented scleroderma or healthy control patients. Tissues samples were fixed in 4% PFA for 24h then conserved on 70% ethanol before processing. Sections were stained with an anti-MPO antibody. Slides for histologic assessment were scanned using a EVOS M7000 microscope (Thermo Fisher Scientific) at 4X magnification. The number of neutrophils was assessed by counting the average number of MPO+ neutrophils from 5 randomly selected fields of view (FOV). Assessment was performed independently by 2 blinded experimenters; data shown reflect the mean of both values.

Mouse skin biopsies were collected from the dorsum of the animals at the injection site. Mouse lungs were inflated before collection via insertion of an intratracheal canula with 4% PFA at a flow rate of 200 µL/second (*82*). Tissue samples were fixed in 4% PFA for 24h then conserved on 70% ethanol before processing. Sections (5 mm thick) of paraffin-embedded samples were stained with Masson's trichrome. Slides for histologic assessment were scanned using a EVOS M7000 microscope (Thermo Fisher Scientific) at 4X magnification. Dermal thickness (layer from

the dermal-epidermal junction to the dermal-adipose junction) was calculated from the average of 3 random measurements per section. For mouse lung fibrosis evaluation, average of multiple FOV of the entire lung were scored according to the modified Ashcroft scale defined by Hübner *et al*. (*32*) The scoring criteria were as follows: (A) Grade 0, normal lung. (B) Grade 1, alveoli partly enlarged and rarefied, absence of fibrotic masses, septum thicker than normal. (C) Grade 2, alveoli partly enlarged and rarefied, absence of fibrotic masses, septum thicker than normal with isolated knot-like formation. (D) Grade 3, alveoli partly enlarged and rarefied, absence of fibrotic masses, septum thicker than normal with continuous fibrotic wall in the entire FOV. (E) Grade 4, single fibrotic masses (≤10% of FOV). (F) Grade 5, single fibrotic masses (10-50% of FOV). (G) Grade 6, large contiguous fibrotic masses (>50% of FOV). (H) Grade 7, alveoli nearly obliterated with fibrous masses but some air bubbles. (I) Grade 8, complete obliteration with fibrotic masses. Mouse skin and lung fibrosis assessment was performed blinded to experimenter using ImageJ software (National Institutes of Health).

Blood collection

Human blood samples were drawn from antecubital veins after providing informed consent, using a 21g butterfly vacutainer tube anticoagulated with citrate or lithium heparin for platelet or neutrophil assessment, respectively. Mouse blood samples were collected as described previously (*83*). Blood was collected from the inferior vena cava of anesthetized animals (isoflurane 1-4%) using a 29g needle attached to a 3mL syringe containing a combination of low molecular weight heparin (enoxaparin, 40 units/ml) and acid-citrate-dextrose (ACD) anticoagulant (13 mM sodium citrate, 1 mM citric acid, 20 mM dextrose, and 10 mM theophylline). For sub-mandibular blood collection, samples were directly collected into heparin tubes.

Neutrophil enumeration in whole blood

Human neutrophil count in heparin-anticoagulated whole blood was assessed using Sysmex XP-300-Hematology-Analyzer.

Human neutrophil isolation

Human neutrophils from blood of healthy donors or dSSc patients were purified with Ficoll-Paque PLUS (Cytiva). Blood was first diluted with PBS (1:1 ratio) and gently layered on top of 15mL of Ficoll-Paque PLUS onto a 50mL falcon tube. The tube was then centrifuged at 500g for 30 minutes at 18°C-22°C without break. The top 3 layers including plasma, PBMC and Ficoll-Paque PLUS, were removed and discarded. The neutrophil layer directly on top of the red blood cells (RBC) and the first portion of the RBC (approximately 1ml) were collected and placed into a clean 50mL falcon tube. RBC were lysed with ACK (GIBCO, 1:20 blood: ACK ratio) for no more than 2 minutes with constant gentle agitation. A solution of PBS containing 2mM EDTA was added to the tube (1:1 ratio) before centrifugation at 500g for 10 minutes at 18°C-22°C. Supernatant was gently removed and neutrophil pellet resuspended in RPMI 1640 (GIBCO). Neutrophil purity was assessed using Sysmex XP-300 automated hematology analyzer.

Mouse neutrophil isolation

Bone marrow murine neutrophils were purified using EasySep™ Mouse Neutrophil Enrichment Kit (STEMCELL technologies) according to the manufacturer's instructions. The purity of neutrophil ($Ly6G^+$ subsets) was assessed by flow cytometry.

T cell isolation

Spleen murine T cells were purified using EasySep™ Mouse T Cell Isolation Kit (STEMCELL technologies) according to the manufacturer's instructions. The purity of T cells, defined as $CD3^+/CD19^-$, was assessed by flow cytometry.

Flow cytometry of neutrophil activation

Human heparin-anticoagulated whole blood was diluted with HBSS (1 volume blood: 4 volume HBSS ratio). Diluted whole blood (100µL) was stained at RT for 30 minutes with antibodies and dyes listed in Supplementary Table 2. Thereafter, RBC were lysed with ACK lysis buffer (1 volume blood: 10 volume ACK) for 1 minutes with gentle agitation, centrifugated at 500g for 5 minutes at 4°C and the pellet resuspended in HBSS. Cell suspension was kept on ice until flow cytometry analysis. We characterized human neutrophil activation by assessing levels of Mac-1^+, L-selectin$^+$, activated Mac-1^+, and ROS (CM-H2DCFDA$^+$) on the neutrophil gated CD66b$^+$ population. Mouse enoxaparin/ACD-anticoagulated whole blood was diluted with HBSS (1 volume blood: 2 volume HBSS ratio). Mouse samples were treated similarly as human samples with specific antibodies and dyes listed in Supplementary Table 2. We characterized mouse neutrophil activation by assessing levels of Mac-1^+, L-selectin$^+$, and ROS (CM-H2DCFDA$^+$) on the neutrophil gated Ly6G$^+$ population. For kinetics of activation in HOCl-SSc mice, whole blood was collected via sub-mandibular vein. For each marker, MFI was obtained by background subtraction obtained from isotype control antibody or unstained samples. All samples were acquired with a BD LSRFortessa™ Cell Analyzer (BD biosciences and recorded data analyzed with FlowJo (v.10.10.0).

Neutrophil migration assay

A volume of 100µL of a suspension of freshly isolated neutrophils (10^6/mL) in RPMI 1640 medium containing 0.1% FBS was placed in the upper compartment of a transwell chamber featuring uncoated polyester membrane with 3 µm pores (Corning), and a volume of 600 µL of RPMI 1640 medium containing 0.1% FBS and LTB4 (100 nM) or vehicle was added to the bottom compartment. After 2 h incubation at 37°C and 5% CO_2, 400 µL were harvested from the bottom compartment and neutrophils, determined as the CD66b$^+$ (human) or Ly6G$^+$ (mouse) population were enumerated by flow cytometry using counting beads.

Flow cytometry of platelet activation in whole blood

Human heparin-anticoagulated whole blood was diluted with Tyrode's buffer (12mM $NaHCO_3$, 10mM HEPES, 137 mM NaCl, 2.7mM KCl, 5.5mM glucose and 1 mM $CaCl_2$/$MgCl_2$, 1 volume blood: 4 volume Tyrode ratio). Diluted whole blood (50 µL) was stained at 37°C for 30 minutes with Antibodies and dyes listed in Supplementary Table 2. Thereafter, samples were diluted with Tyrode's buffer (1 volume of blood: 10 volume of buffer ratio) before examination by flow cytometry. We characterized platelet activation as follows: CD41$^+$-P-selectin$^+$-Annexin V$^+$. Mouse enoxaparin-anticoagulated whole blood was diluted with Tyrode's buffer supplemented with 1 mM $CaCl_2$/$MgCl_2$ (1 volume blood: 2 volume Tyrode ratio) and treated similarly as human whole blood. For kinetics of activation in HOCl-SSc mice, whole blood was collected via sub-mandibular vein.

For each marker, MFI was obtained by background subtraction obtained from isotype control antibody or unstained samples when applicable. All samples were acquired with a BD LSRFortessa™ Cell Analyzer (BD biosciences and recorded data analyzed with FlowJo (v.10.10.0).

Preparation of washed platelets and examination of activation profile by flow cytometry

Human or murine washed platelets were prepared as described (*84*) with slight modifications. Anti-coagulated blood was diluted with platelet washing buffer, PWB (4.3 mM Na_2HPO, 24.3 mM NaH_2PO, 4.3 mM K_2HPO_4, 113 mM NaCl, 5.5 mM glucose, 0.5% BSA, and 10 mM theophylline, pH 6.5, 1:1 ratio) containing enoxaparin (20 U/ml clexane) and apyrase (0.01 U/ml). Diluted platelet-rich plasma (PRP) was obtained by centrifugation at 37°C for 5 mins at 250g without break. Platelets in diluted PRP were then pelleted by centrifugation at 2000 x g for 5 mins at

37°C and washed twice in PWB and then finally resuspended (10^6/mL) in Tyrode's buffer (10 mM Hepes, 12 mM $NaHCO_3$, 137 mM NaCl, 2.7 mM KCl, 5 mM glucose, pH 7.4) supplemented with 1 mM $CaCl_2$/$MgCl_2$ and 0.02 U/ml Apyrase. Platelets were let rest for 30 mins at 37°C, before stimulation and staining. We characterized P-selectin and Annexin V expression on singlet CD41+ population. All samples were acquired with a BD LSRFortessa™ Cell Analyzer (BD biosciences and recorded data analyzed with FlowJo (v.10.10.0).

Whole lung homogenization

Whole lung samples were perfused and collected onto a 15mL falcon tube containing 500 µL of tissue protein extraction buffer (Pierce T-PER™, Tissue Protein Extraction Reagent, Thermo Fisher Scientific) containing protease (cOmplete™, EDTA-free Protease Inhibitor Cocktail) and phosphatase (PhosSTOP™) inhibitors. Samples were submitted to homogenization at maximum speed for 1 minutes on ice (Fisherbrand™ 150 Handheld Homogenizer). Thereafter, samples were transferred to a clean microcentrifuge tube and centrifuged at 16,000 × g for 10 mins at 4°C. Supernatant was collected to a new microcentrifuge tube and stored at -80°C until analysis.

NETs formation and quantification *in vitro*

Freshly isolated neutrophils (1 x 10^6) in RPMI containing 10% FBS were seeded onto a 24-well plate and stimulated with vehicle, A23187 (5 µM), or platelets (ratio 1 neutrophil: 50 platelets) for 3 or 4 h, human or mouse, respectively. Thereafter, each well was washed twice to removed unbound DNA before applying a solution of S7 nuclease (50 U/ml) in RPMI containing 10% FBS and incubation at 37°C for 30 minutes. The supernatant containing DNA and citrullinated H3 (citH3) was then transferred onto a microcentrifuge tube containing EDTA (5mM final) and centrifuged 5 minutes at 300g without break. The supernatant was then collected onto a clean microcentrifuge tube and stored at -80°C until analysis. Quantification of citH3 was performed on collected samples using the Citrullinated Histone H3 (Clone 11D3) ELISA Kit (Cayman Chemicals) according to manufacturer's instructions. Absorbance at 450 nm was measured using a Synergy HTX multi-mode microplate reader.

NET quantification *in vivo*

NETosis was determined as the quantity of citrullinated histone H3 (CitH3) detected in mouse sera (1:2 dilution) or lung tissue homogenates with the citrullinated histone H3 ELISA kit (Cayman Chemical).

Neutrophil count in bronchoalveolar lavage and lung

Bronchoalveolar lavage (BAL) fluid was collected on euthanized mice via isoflurane overdose by gently washing the lungs with 1 ml sterile PBS for three times in the bronchial tree using a 22g endotracheal tube (Kent scientific). Lungs were then perfused at a rate of 200µL/second using a 3mL syringe with a 22g needle containing PBS into the right ventricle of the heart. Approximatively 2.5mL of PBS are generally used per lung. Whole lung samples were then harvested and submitted to enzymatic digestion in RPMI 1640 containing collagenase 2 (2mg/mL) and DNAse I (0.1 mg/mL) for 30 minutes at 37°C under constant mixing at 900 rpm in a thermomixer (Eppendorf® Thermomixer). After digestion, lung samples were submitted to a 70mM cell strainer on ice. Resulting cell suspensions from BAL and whole lung digestion were centrifuged at 500g for 5 mins at 4°C and resuspended with PBS/0.5% BSA before staining for neutrophils (anti-Ly6G antibody). Ly6G+ population was quantified by flow cytometry as percentage of all cells or absolute count using counting beads.

Neutrophil depletion

Neutrophil were depleted using anti-mouse Ly6G (clone 1A8, BioXCell) injected in i.p at 100 μg for 7 consecutive days following by an injection every second day until the experiment end. For each experiment, rat IgG2a isotype control, anti-trinitrophenol (clone 2A3, BioXCell) was used as control. Neutrophil depletion efficiency was assessed by flow cytometry identified in the $CD45^{+}/Ly6C^{+}$ quadrant.

Platelet depletion

For diphtheria toxin (DT)-induced platelet depletion, $PF4^{Cre+}/DTR^{fl/fl}$ and $PF4^{Cre-}/DTR^{fl/fl}$ (control) mice received i.p. injection of 250 ng of DT for 7 consecutive days following by an injection every three day until the experiment end. Platelet depletion in whole blood collected via the submandibular vein was assessed using Sysmex XP-300-Hematology-Analyzer.

Adoptive transfer

Neutrophils were isolated from the bone marrow, T cell were isolated from the spleen, platelets were isolated from the blood. For platelet-activated neutrophils experiments, neutrophils were co-culture with platelets (ratio 1 neutrophil to 50 platelets) at 37°C for 3 h prior to treatment with trypsin/EDTA (0.01%) and centrifugation at 300g for 5 minutes to remove platelets prior neutrophil injection. Cells (5×10^{6}) were injected i.d (skin fibrosis) or i.v. (lung fibrosis) into a recipient mouse. Tissues were collected after 14 days before tissue collection and processing as described above.

Detection of Scl-70 in the serum

Anti–Scl-70 antibodies were detected in mouse sera (1:4 dilution) using a mouse anti-Scl-70 ELISA kit (Signosis) following manufacturer's instruction. Absorbance at 450 nm was measured using a Synergy HTX multi-mode microplate reader.

Total collagen content in lung

Total collagen content in lung was measured from whole lung homogenate using the total collagen assay kit (Quickzyme Biosciences). Results were expressed as the total collagen content in lung (mg/whole lung).

Transcriptomic data

Acquisition of Transcriptomic Data

Publicly available microarray or RNA-sequencing data from patients with SSC and healthy controls were retrieved from the NCBI's Gene Expression Omnibus (GEO) using the R package GEOquery. A total of eight GEO data sets generated from lung biopsy, skin biopsy, or whole blood samples were included in the SSC meta-analysis data set for the transcriptomic analysis. The accession numbers and general statistics are included in Supplemental Figure 2B.

Integration of GEO Datasets

Integration of the GEO discovery sets was performed using the R packages MetaIntegrator and COCONUT[80] to allow for analysis of the eight studies as a single batch-corrected transcriptomic data set. The COCONUT algorithm applies batch correction to all control samples to achieve a common baseline, then uses the correction parameters obtained in the control batch correction to non-control samples to create a transcriptomic dataset for meta-analysis with minimal batch effects.

Differential Gene Expression and Gene Set Enrichment Analysis

The limma[91] pipeline was used to perform differential gene expression analysis and rotation gene set testing for selected gene sets. Gene sets were created from published gene signatures

of interest or retrieved from the REACTOME database. Multiple testing correction was applied to the three gene set roast results and false discovery rate is reported as a significance measure. Pathway analysis of the meta-dataset was performed using the fgsea R package[92] with REACTOMEdb gene modules. Results from differential gene expression analysis were ranked on log fold-change for input into the fgsea algorithm. A separate pathway overrepresentation analysis was performed on the REACTOME analysis platform with significantly upregulated and downregulated DEGs to confirm the fgsea results.

Quantification and statistical analysis

Results were analyzed with GraphPad Prism statistical software (version 10.1.1). The statistical tests used are specified in the figure legends. Two-tailed unpaired t-tests were performed when comparing only two groups, Paired t-tests were used to compare internally controlled replicates, and ordinary one- and two-way ANOVA using Turkey's multiple comparisons test was performed when comparing one variable across multiple groups. Sample sizes for each experiment are provided in the figures and the respective legends. P values are indicated in each figure.

ACKNOWLEDGMENTS

R.D. was supported by an Arthritis National Research Foundation (ANRF) award, a National Scleroderma Research Foundation New Investigator Grant, and NIH/NIAMS P30 AR070253 pilot grants. L.S. was supported by NIH/NIAID T32 AI007512. M.G.A. was supported by NIH P30AR070253, the ARNF, the Viv Braden family, and the Lupus Research Alliance. P.A.J. was supported by PHOCEO AP-HM, Philippe Foundation, and Association France Vascularites. D.W. was supported by NIH/NHLBI R35HL166556**.** SBM was supported by NIH/NHLBI K23HL150331 and R01HL171240. P.A.N. was supported by NIH/NIAMS 2R01AR065538, R01AR075906, R01AR073201, P30AR070253, a Global Team Science Award from the Lupus Research Alliance, and the Be Brave Foundation.

REFERENCES

1. T. R. Katsumoto, M. L. Whitfield, M. K. Connolly, The pathogenesis of systemic sclerosis. *Annu Rev Pathol* **6**, 509-537 (2011).
2. M. Zeisberg, R. Kalluri, Cellular mechanisms of tissue fibrosis. 1. Common and organ-specific mechanisms associated with tissue fibrosis. *Am J Physiol Cell Physiol* **304**, C216-225 (2013).
3. J. A. Varga, M. Trojanowska, Fibrosis in systemic sclerosis. *Rheum Dis Clin North Am* **34**, 115-143; vii (2008).
4. S. Panopoulos, V. K. Bournia, G. Konstantonis, K. Fragiadaki, P. P. Sfikakis, M. G. Tektonidou, Predictors of morbidity and mortality in early systemic sclerosis: Long-term follow-up data from a single-centre inception cohort. *Autoimmun Rev* **17**, 816-820 (2018).
5. T. A. Wynn, Cellular and molecular mechanisms of fibrosis. *J Pathol* **214**, 199-210 (2008).
6. M. Brown, S. O'Reilly, The immunopathogenesis of fibrosis in systemic sclerosis. *Clin Exp Immunol* **195**, 310-321 (2019).
7. W. Jin, Y. Zheng, P. Zhu, T cell abnormalities in systemic sclerosis. *Autoimmun Rev* **21**, 103185 (2022).
8. L. I. Sakkas, D. P. Bogdanos, Systemic sclerosis: New evidence re-enforces the role of B cells. *Autoimmun Rev* **15**, 155-161 (2016).

9. A. Lescoat, V. Lecureur, J. Varga, Contribution of monocytes and macrophages to the pathogenesis of systemic sclerosis: recent insights and therapeutic implications. *Curr Opin Rheumatol* **33**, 463-470 (2021).
10. O. Kowal-Bielecka, K. Kowal, K. B. Highland, R. M. Silver, Bronchoalveolar lavage fluid in scleroderma interstitial lung disease: technical aspects and clinical correlations: review of the literature. *Semin Arthritis Rheum* **40**, 73-88 (2010).
11. A. U. Wells, D. M. Hansell, M. B. Rubens, P. Cullinan, P. L. Haslam, C. M. Black, R. M. D. Bois, Fibrosing alveolitis in systemic sclerosis. Bronchoalveolar lavage findings in relation to computed tomographic appearance. *American Journal of Respiratory and Critical Care Medicine* **150**, 462-468 (1994).
12. N. Wareing, V. Mohan, R. Taherian, E. R. Volkmann, M. A. Lyons, H. Wilhalme, M. D. Roth, Y. M. R. M. Estrada, B. Skaug, M. D. Mayes, D. P. Tashkin, S. Assassi, Blood Neutrophil Count and Neutrophil-to-Lymphocyte Ratio for Prediction of Disease Progression and Mortality in Two Independent Systemic Sclerosis Cohorts. *Arthritis Care Res (Hoboken)* **75**, 648-656 (2023).
13. D. Impellizzieri, C. Egholm, A. Valaperti, O. Distler, O. Boyman, Patients with systemic sclerosis show phenotypic and functional defects in neutrophils. *Allergy* **77**, 1274-1284 (2022).
14. R. Kuley, R. D. Stultz, B. Duvvuri, T. Wang, M. J. Fritzler, R. Hesselstrand, J. L. Nelson, C. Lood, N-Formyl Methionine Peptide-Mediated Neutrophil Activation in Systemic Sclerosis. *Front Immunol* **12**, 785275 (2021).
15. C. L. Maslen, N. D. Hall, A. D. Woolf, P. J. Maddison, Enhanced oxidative metabolism of neutrophils from patients with systemic sclerosis. *Br J Rheumatol* **26**, 113-117 (1987).
16. N. Maugeri, P. Rovere-Querini, M. Baldini, E. Baldissera, M. G. Sabbadini, M. E. Bianchi, A. A. Manfredi, Oxidative stress elicits platelet/leukocyte inflammatory interactions via HMGB1: a candidate for microvessel injury in sytemic sclerosis. *Antioxid Redox Signal* **20**, 1060-1074 (2014).
17. T. C. Barnes, M. E. Anderson, S. W. Edwards, R. J. Moots, Neutrophil-derived reactive oxygen species in SSc. *Rheumatology* **51**, 1166-1169 (2012).
18. M. Matucci-Cerinic, B. Kahaleh, F. M. Wigley, Review: evidence that systemic sclerosis is a vascular disease. *Arthritis Rheum* **65**, 1953-1962 (2013).
19. S. Piera-Velazquez, P. J. Wermuth, J. J. Gomez-Reino, J. Varga, S. A. Jimenez, Chemical exposure-induced systemic fibrosing disorders: Novel insights into systemic sclerosis etiology and pathogenesis. *Semin Arthritis Rheum* **50**, 1226-1237 (2020).
20. Y. Asano, The Pathogenesis of Systemic Sclerosis: An Understanding Based on a Common Pathologic Cascade across Multiple Organs and Additional Organ-Specific Pathologies. *J Clin Med* **9**, (2020).
21. J. Ko, M. Noviani, V. R. Chellamuthu, S. Albani, A. H. L. Low, The Pathogenesis of Systemic Sclerosis: The Origin of Fibrosis and Interlink with Vasculopathy and Autoimmunity. *International Journal of Molecular Sciences* **24**, 14287 (2023).
22. H. Yasuoka, K. Sakata, K. Yoshimoto, T. Takeuchi, Phenotype of Platelets Are Altered and Activated in Circulation of Patients with Systemic Sclerosis. *Blood* **132**, 3732 (2018).
23. A. Solanilla, J. Villeneuve, P. Auguste, M. Hugues, A. Alioum, S. Lepreux, J.-P. Ducroix, P. Duhaut, C. Conri, J.-F. Viallard, A. T. Nurden, J. Constans, J. Ripoche, The transport of high amounts of vascular endothelial growth factor by blood platelets underlines their potential contribution in systemic sclerosis angiogenesis. *Rheumatology* **48**, 1036-1044 (2009).
24. G. E. Pamuk, B. Turgut, O. N. Pamuk, O. Vural, M. Demir, N. Cakir, Increased circulating platelet-leucocyte complexes in patients with primary Raynaud's phenomenon and Raynaud's phenomenon secondary to systemic sclerosis: a comparative study. *Blood Coagul Fibrinolysis* **18**, 297-302 (2007).

25. G. A. Ramirez, S. Franchini, P. Rovere-Querini, M. G. Sabbadini, A. A. Manfredi, N. Maugeri, The role of platelets in the pathogenesis of systemic sclerosis. *Front Immunol* **3**, 160 (2012).
26. M. J. Goodfield, M. A. Orchard, N. R. Rowell, Increased platelet sensitivity to collagen-induced aggregation in whole blood patients with systemic sclerosis. *Clin Exp Rheumatol* **6**, 285-288 (1988).
27. M. B. Kahaleh, K. K. Scharstein, E. C. LeRoy, Enhanced platelet adhesion to collagen in scleroderma. Effect of scleroderma plasma and scleroderma platelets. *J Rheumatol* **12**, 468-471 (1985).
28. M. J. D. Goodfield, M. A. Orchard, N. R. Rowell, Whole blood platelet aggregation and coagulation factors in patients with systemic sclerosis. *British Journal of Haematology* **84**, 675-680 (1993).
29. N. Maugeri, A. Capobianco, P. Rovere-Querini, G. A. Ramirez, E. Tombetti, P. D. Valle, A. Monno, V. D'Alberti, A. M. Gasparri, S. Franchini, A. D'Angelo, M. E. Bianchi, A. A. Manfredi, Platelet microparticles sustain autophagy-associated activation of neutrophils in systemic sclerosis. *Sci Transl Med* **10**, (2018).
30. A. T. Maria, K. Toupet, C. Bony, N. Pirot, M. C. Vozenin, B. Petit, P. Roger, F. Batteux, A. Le Quellec, C. Jorgensen, D. Noël, P. Guilpain, Antifibrotic, Antioxidant, and Immunomodulatory Effects of Mesenchymal Stem Cells in HOCl-Induced Systemic Sclerosis. *Arthritis Rheumatol* **68**, 1013-1025 (2016).
31. T. Yamamoto, S. Takagawa, I. Katayama, K. Yamazaki, Y. Hamazaki, H. Shinkai, K. Nishioka, Animal model of sclerotic skin. I: Local injections of bleomycin induce sclerotic skin mimicking scleroderma. *J Invest Dermatol* **112**, 456-462 (1999).
32. R. H. Hübner, W. Gitter, N. E. El Mokhtari, M. Mathiak, M. Both, H. Bolte, S. Freitag-Wolf, B. Bewig, Standardized quantification of pulmonary fibrosis in histological samples. *Biotechniques* **44**, 507-511, 514-507 (2008).
33. A. T. J. Maria, K. Toupet, M. Maumus, P. Rozier, M. C. Vozenin, A. Le Quellec, C. Jorgensen, D. Noël, P. Guilpain, Fibrosis Development in HOCl-Induced Systemic Sclerosis: A Multistage Process Hampered by Mesenchymal Stem Cells. *Front Immunol* **9**, 2571 (2018).
34. B. Peng, Q. Hu, R. He, H. Hou, D. Lian, Y. Chen, H. Li, L. Song, Y. Gao, T. Chen, G. Zhang, J. Li, Baicalein alleviates fibrosis and inflammation in systemic sclerosis by regulating B-cell abnormalities. *BMC Complement Med Ther* **23**, 62 (2023).
35. C. Kayser, M. J. Fritzler, Autoantibodies in Systemic Sclerosis: Unanswered Questions. *Frontiers in Immunology* **6**, (2015).
36. X. Li, S. Xiao, N. Filipczak, S. S. K. Yalamarty, H. Shang, J. Zhang, Q. Zheng, Role and Therapeutic Targeting Strategies of Neutrophil Extracellular Traps in Inflammation. *Int J Nanomedicine* **18**, 5265-5287 (2023).
37. R. M. Adel, H. Helal, M. Ahmed Fouad, S. Sobhy Abd-Elhalem, Regulation of miRNA-155-5p ameliorates NETosis in pulmonary fibrosis rat model via inhibiting its target cytokines IL-1β, TNF-α and TGF-β1. *Int Immunopharmacol* **127**, 111456 (2024).
38. C. G. McCarthy, P. Saha, R. M. Golonka, C. F. Wenceslau, B. Joe, M. Vijay-Kumar, Innate Immune Cells and Hypertension: Neutrophils and Neutrophil Extracellular Traps (NETs). *Compr Physiol* **11**, 1575-1589 (2021).
39. S. Shrestha, C. W. Hong, Extracellular Mechanisms of Neutrophils in Immune Cell Crosstalk. *Immune Netw* **23**, e38 (2023).
40. W. Wang, Z. Liu, Y. Zhang, L. Wang, D. Meng, X. Li, J. Zhang, Y. Wu, X. Zhou, G. Liu, Benzyl butyl phthalate (BBP) induces lung injury and fibrosis through neutrophil extracellular traps. *Environ Pollut* **309**, 119743 (2022).

41. L. He, R. Liu, H. Yue, X. Zhang, X. Pan, Y. Sun, J. Shi, G. Zhu, C. Qin, Y. Guo, Interaction between neutrophil extracellular traps and cardiomyocytes contributes to atrial fibrillation progression. *Signal Transduct Target Ther* **8**, 279 (2023).
42. Z. Wu, X. Chen, S. Wu, Z. Liu, H. Li, K. Mai, Y. Peng, H. Zhang, X. Zhang, Z. Zheng, Z. Fu, D. Chen, Transcriptome analysis reveals the impact of NETs activation on airway epithelial cell EMT and inflammation in bronchiolitis obliterans. *Sci Rep* **13**, 19226 (2023).
43. E. Pieterse, N. Rother, M. Garsen, J. M. Hofstra, S. C. Satchell, M. Hoffmann, M. A. Loeven, H. K. Knaapen, O. W. H. van der Heijden, J. H. M. Berden, L. B. Hilbrands, J. van der Vlag, Neutrophil Extracellular Traps Drive Endothelial-to-Mesenchymal Transition. *Arterioscler Thromb Vasc Biol* **37**, 1371-1379 (2017).
44. L. Pandolfi, S. Bozzini, V. Frangipane, E. Percivalle, A. De Luigi, M. B. Violatto, G. Lopez, E. Gabanti, L. Carsana, M. D'Amato, M. Morosini, M. De Amici, M. Nebuloni, T. Fossali, R. Colombo, L. Saracino, V. Codullo, M. Gnecchi, P. Bigini, F. Baldanti, D. Lilleri, F. Meloni, Neutrophil Extracellular Traps Induce the Epithelial-Mesenchymal Transition: Implications in Post-COVID-19 Fibrosis. *Front Immunol* **12**, 663303 (2021).
45. A. Chrysanthopoulou, I. Mitroulis, E. Apostolidou, S. Arelaki, D. Mikroulis, T. Konstantinidis, E. Sivridis, M. Koffa, A. Giatromanolaki, D. T. Boumpas, K. Ritis, K. Kambas, Neutrophil extracellular traps promote differentiation and function of fibroblasts. *J Pathol* **233**, 294-307 (2014).
46. S. Zhang, X. Jia, Q. Zhang, L. Zhang, J. Yang, C. Hu, J. Shi, X. Jiang, J. Lu, H. Shen, Neutrophil extracellular traps activate lung fibroblast to induce polymyositis-related interstitial lung diseases via TLR9-miR-7-Smad2 pathway. *J Cell Mol Med* **24**, 1658-1669 (2020).
47. R. Molinaro, M. Yu, G. Sausen, C. A. Bichsel, C. Corbo, E. J. Folco, G. Y. Lee, Y. Liu, Y. Tesmenitsky, E. Shvartz, G. K. Sukhova, F. Kloss, K. J. Croce, O. C. Farokhzad, J. Shi, P. Libby, Targeted delivery of protein arginine deiminase-4 inhibitors to limit arterial intimal NETosis and preserve endothelial integrity. *Cardiovasc Res* **117**, 2652-2663 (2021).
48. K. Daigo, N. Yamaguchi, T. Kawamura, K. Matsubara, S. Jiang, R. Ohashi, Y. Sudou, T. Kodama, M. Naito, K. Inoue, T. Hamakubo, The proteomic profile of circulating pentraxin 3 (PTX3) complex in sepsis demonstrates the interaction with azurocidin 1 and other components of neutrophil extracellular traps. *Mol Cell Proteomics* **11**, M111.015073 (2012).
49. T. A. Fuchs, U. Abed, C. Goosmann, R. Hurwitz, I. Schulze, V. Wahn, Y. Weinrauch, V. Brinkmann, A. Zychlinsky, Novel cell death program leads to neutrophil extracellular traps. *J Cell Biol* **176**, 231-241 (2007).
50. Y. Wang, M. Li, S. Stadler, S. Correll, P. Li, D. Wang, R. Hayama, L. Leonelli, H. Han, S. A. Grigoryev, C. D. Allis, S. A. Coonrod, Histone hypercitrullination mediates chromatin decondensation and neutrophil extracellular trap formation. *J Cell Biol* **184**, 205-213 (2009).
51. V. Sreeramkumar, J. M. Adrover, I. Ballesteros, M. I. Cuartero, J. Rossaint, I. Bilbao, M. Nácher, C. Pitaval, I. Radovanovic, Y. Fukui, R. P. McEver, M.-D. Filippi, I. Lizasoain, J. Ruiz-Cabello, A. Zarbock, M. A. Moro, A. Hidalgo, Neutrophils scan for activated platelets to initiate inflammation. *Science* **346**, 1234-1238 (2014).
52. K. N. Kornerup, G. P. Salmon, S. C. Pitchford, W. L. Liu, C. P. Page, Circulating platelet-neutrophil complexes are important for subsequent neutrophil activation and migration. *Journal of Applied Physiology* **109**, 758-767 (2010).
53. R. Polanowska-Grabowska, K. Wallace, J. J. Field, L. Chen, M. A. Marshall, R. Figler, A. R. L. Gear, J. Linden, P-Selectin–Mediated Platelet-Neutrophil Aggregate

Formation Activates Neutrophils in Mouse and Human Sickle Cell Disease*. *Arteriosclerosis, Thrombosis, and Vascular Biology* **30**, 2392-2399 (2010).
54. L. M. Wuescher, S. Nishat, R. G. Worth, Characterization of a transgenic mouse model of chronic conditional platelet depletion. *Research and Practice in Thrombosis and Haemostasis* **3**, 704-712 (2019).
55. N. Li, H. Hu, M. Lindqvist, E. Wikström-Jonsson, A. H. Goodall, P. Hjemdahl, Platelet-Leukocyte Cross Talk in Whole Blood. *Arteriosclerosis, Thrombosis, and Vascular Biology* **20**, 2702-2708 (2000).
56. J. Pircher, B. Engelmann, S. Massberg, C. Schulz, Platelet–Neutrophil Crosstalk in Atherothrombosis. *Thromb Haemost* **119**, 1274-1282 (2019).
57. S. A. Jimenez, C. T. Derk, Following the molecular pathways toward an understanding of the pathogenesis of systemic sclerosis. *Ann Intern Med* **140**, 37-50 (2004).
58. Y. Asano, The Pathogenesis of Systemic Sclerosis: An Understanding Based on a Common Pathologic Cascade across Multiple Organs and Additional Organ-Specific Pathologies. *Journal of Clinical Medicine* **9**, 2687 (2020).
59. M. M. Cerinic, G. Valentini, G. G. Sorano, S. D'Angelo, G. Cuomo, L. Fenu, S. Generini, S. Cinotti, M. Morfini, A. Pignone, S. Guiducci, A. Del Rosso, R. Kalfin, D. Das, F. Marongiu, Blood coagulation, fibrinolysis, and markers of endothelial dysfunction in systemic sclerosis. *Semin Arthritis Rheum* **32**, 285-295 (2003).
60. J. Etulain, K. Martinod, S. L. Wong, S. M. Cifuni, M. Schattner, D. D. Wagner, P-selectin promotes neutrophil extracellular trap formation in mice. *Blood* **126**, 242-246 (2015).
61. C. Dees, A. Akhmetshina, P. Zerr, N. Reich, K. Palumbo, A. Horn, A. Jüngel, C. Beyer, G. Krönke, J. Zwerina, R. Reiter, N. Alenina, L. Maroteaux, S. Gay, G. Schett, O. Distler, J. H. W. Distler, Platelet-derived serotonin links vascular disease and tissue fibrosis. *Journal of Experimental Medicine* **208**, 961-972 (2011).
62. V. Matus, G. Valenzuela, C. G. Sáez, P. Hidalgo, M. Lagos, E. Aranda, O. Panes, J. Pereira, X. Pillois, A. T. Nurden, D. Mezzano, An adenine insertion in exon 6 of human GP6 generates a truncated protein associated with a bleeding disorder in four Chilean families. *J Thromb Haemost* **11**, 1751-1759 (2013).
63. J. F. Arthur, S. Dunkley, R. K. Andrews, Platelet glycoprotein VI-related clinical defects. *Br J Haematol* **139**, 363-372 (2007).
64. A. Slater, S. Khattak, M. R. Thomas, GPVI inhibition: Advancing antithrombotic therapy in cardiovascular disease. *European Heart Journal - Cardiovascular Pharmacotherapy*, (2024).
65. T. Uphaus, T. Richards, C. Weimar, H. Neugebauer, S. Poli, K. Weissenborn, C. Imray, D. Michalski, H. Rashid, I. Loftus, C. Rummey, M. Ritter, T.-K. Hauser, G. Münch, K. Gröschel, H. Poppert, Revacept, an Inhibitor of Platelet Adhesion in Symptomatic Carotid Stenosis: A Multicenter Randomized Phase II Trial. *Stroke* **53**, 2718-2729 (2022).
66. S. Wichaiyo, W. Parichatikanond, W. Rattanavipanon, Glenzocimab: A GPVI (Glycoprotein VI)-Targeted Potential Antiplatelet Agent for the Treatment of Acute Ischemic Stroke. *Stroke* **53**, 3506-3513 (2022).
67. M. Suzuki, J. Ikari, R. Anazawa, N. Tanaka, Y. Katsumata, A. Shimada, E. Suzuki, K. Tatsumi, PAD4 Deficiency Improves Bleomycin-induced Neutrophil Extracellular Traps and Fibrosis in Mouse Lung. *American Journal of Respiratory Cell and Molecular Biology* **63**, 806-818 (2020).
68. K. Martinod, T. Witsch, L. Erpenbeck, A. Savchenko, H. Hayashi, D. Cherpokova, M. Gallant, M. Mauler, S. M. Cifuni, D. D. Wagner, Peptidylarginine deiminase 4 promotes age-related organ fibrosis. *J Exp Med* **214**, 439-458 (2017).
69. A. Rohrbach, D. Slade, P. Thompson, K. Mowen, Activation of PAD4 in NET formation. *Frontiers in Immunology* **3**, (2012).

70. S. Mohanan, S. Horibata, J. L. McElwee, A. J. Dannenberg, S. A. Coonrod, Identification of macrophage extracellular trap-like structures in mammary gland adipose tissue: a preliminary study. *Front Immunol* **4**, 67 (2013).
71. S. J. Bashar, C. L. Holmes, M. A. Shelef, Macrophage extracellular traps require peptidylarginine deiminase 2 and 4 and are a source of citrullinated antigens bound by rheumatoid arthritis autoantibodies. *Frontiers in Immunology* **15**, (2024).
72. Y. Al-Adwi, J. Westra, H. van Goor, J. K. Burgess, C. P. Denton, D. J. Mulder, Macrophages as determinants and regulators of fibrosis in systemic sclerosis. *Rheumatology* **62**, 535-545 (2022).
73. R. Bhandari, M. S. Ball, V. Martyanov, D. Popovich, E. Schaafsma, S. Han, M. ElTanbouly, N. M. Orzechowski, M. Carns, E. Arroyo, K. Aren, M. Hinchcliff, M. L. Whitfield, P. A. Pioli, Profibrotic Activation of Human Macrophages in Systemic Sclerosis. *Arthritis & Rheumatology* **72**, 1160-1169 (2020).
74. H. Deng, C. Lin, L. Garcia-Gerique, S. Fu, Z. Cruz, E. E. Bonner, M. Rosenwasser, S. Rajagopal, M. N. Sadhu, C. Gajendran, M. Zainuddin, R. Gosu, D. Sivanandhan, M. A. Shelef, B. Nam, D. T. Vogl, D. I. Gabrilovich, Y. Nefedova, A Novel Selective Inhibitor JBI-589 Targets PAD4-Mediated Neutrophil Migration to Suppress Tumor Progression. *Cancer Research* **82**, 3561-3572 (2022).
75. Y. Jia, R. Jia, A. Taledaohan, Y. Wang, Y. Wang, Structure-Activity Relationship of PAD4 Inhibitors and Their Role in Tumor Immunotherapy. *Pharmaceutics* **16**, (2024).
76. C. Gajendran, S. Fukui, N. M. Sadhu, M. Zainuddin, S. Rajagopal, R. Gosu, S. Gutch, S. Fukui, C. E. Sheehy, L. Chu, S. Vishwakarma, D. A. Jeyaraj, G. Hallur, D. D. Wagner, D. Sivanandhan, Alleviation of arthritis through prevention of neutrophil extracellular traps by an orally available inhibitor of protein arginine deiminase 4. *Scientific Reports* **13**, 3189 (2023).
77. W. Elliott, Jr., M. R. Guda, S. Asuthkar, N. Teluguakula, D. V. R. Prasad, A. J. Tsung, K. K. Velpula, PAD Inhibitors as a Potential Treatment for SARS-CoV-2 Immunothrombosis. *Biomedicines* **9**, (2021).
78. D. J. Rabbolini, E. E. Gardiner, M. C. Morel-Kopp, S. Dunkley, A. Jahangiri, C. S. Lee, W. S. Stevenson, C. M. Ward, Anti-glycoprotein VI mediated immune thrombocytopenia: An under-recognized and significant entity? *Res Pract Thromb Haemost* **1**, 291-295 (2017).
79. B. Boylan, H. Chen, V. Rathore, C. Paddock, M. Salacz, K. D. Friedman, B. R. Curtis, M. Stapleton, D. K. Newman, M. L. Kahn, P. J. Newman, Anti-GPVI-associated ITP: an acquired platelet disorder caused by autoantibody-mediated clearance of the GPVI/FcRgamma-chain complex from the human platelet surface. *Blood* **104**, 1350-1355 (2004).
80. H. Takahashi, M. Moroi, Antibody against platelet membrane glycoprotein VI in a patient with systemic lupus erythematosus. *Am J Hematol* **67**, 262-267 (2001).
81. A. I. Servettaz, C. Goulvestre, N. Kavian, C. Nicco, P. Guilpain, C. Chéreau, V. Vuiblet, L. c. Guillevin, L. Mouthon, B. Weill, F. d. r. Batteux, Selective Oxidation of DNA Topoisomerase 1 Induces Systemic Sclerosis in the Mouse1. *The Journal of Immunology* **182**, 5855-5864 (2009).
82. M. L. Davenport, T. P. Sherrill, T. S. Blackwell, M. D. Edmonds, Perfusion and Inflation of the Mouse Lung for Tumor Histology. *J Vis Exp*, (2020).
83. M. J. Maxwell, Y. Yuan, K. E. Anderson, M. L. Hibbs, H. H. Salem, S. P. Jackson, SHIP1 and Lyn Kinase Negatively Regulate Integrin alpha IIb beta 3 signaling in platelets. *J Biol Chem* **279**, 32196-32204 (2004).
84. S. P. Jackson, S. M. Schoenwaelder, Y. Yuan, I. Rabinowitz, H. H. Salem, C. A. Mitchell, Adhesion receptor activation of phosphatidylinositol 3-kinase. von Willebrand factor

stimulates the cytoskeletal association and activation of phosphatidylinositol 3-kinase and pp60c-src in human platelets. *J Biol Chem* **269**, 27093-27099 (1994).

FIGURE LEGENDS

FIGURE 1. Neutrophils exhibit an activated phenotype in human dSSc.
(A-C) Complete blood count (CBC) was performed in 12 healthy controls (HC) and 12 diffuse systemic sclerosis (dSSc) patients. Neutrophil count ($x10^3$/mL) in whole blood of HC and dSSc patients. **(B)** Proportion of neutrophils among total white blood cells (WBC) in HC and patients with dSSc. **(C)** Neutrophil-to-Lymphocyte ratio in HC and dSSc patients. **(D-G)** Whole blood neutrophils from dSSc patients or healthy controls were assayed by flow cytometry. Representative histogram plot (left) and quantification (right) showing expression of the indicated markers in neutrophils from HC and dSSc patients (n=10 per group). **(H)** Neutrophils from HC and dSSc patients (n= 7/group) were assayed for their migration capacity toward the chemoattractant LTB_4. Data are expressed as fold increased over no LTB_4. Each dot is the average of duplicates for each condition. **(I)** Enhanced volcano plot of genes differentially expressed between HC and dSSc patients. The x and y axes indicate the expression fold change (FC) (log2) and the false discovery rate (FDR) (−log10) for each dSSc gene versus control. Legends highlight upregulated or downregulated transcripts (red), cutoff criteria for fold-change of 0.5 and the Benjamini-Hochberg FDR corrected p-value of 0.05. **(J)** Bar plots showing the normalized enrichment score (NES) of selected gene ontology categories within genes upregulated (red) or downregulated (blue) in pooled dataset from lungs, skin and blood from the dSSc compared to control patients. Neutrophil (red arrow) and platelet (red arrowhead) pathways are shown. The data represent the mean ± SD. ROS, reactive oxygen species; FMO, fluorescence minus one.

FIGURE 2. HOCl-SSc and BLM-SSc models recapitulate aspects of human dSSc.
(A) Representative skin sections (left) of a control skin (PBS) compared to back skin from a d42 and a d28 HOCl- and BLM-SSc mouse (original magnification 4x; Masson Trichrome staining). Dermal thickness (right) was measured for each group (HOCl model: n = 10 PBS and n =11 HOCl; BLM model: n= 13 PBS and n=13 BLM). **(B)** Representative lung sections (left) of a control lung (PBS) compared to lung from d42 and a d28 HOCl- and BLM-SSc mice, respectively (original magnification 20x; Masson Trichrome staining). Microscopic scores of lung sections according to a modified Ashcroft's method (right) were determined for each group (HOCl model: n = 10 PBS and n =11 HOCl; BLM model: n= 13 PBS and n=13 BLM). **(C)** Total collagen content in the lung from PBS-, HOCl- or BLM-treated mice (n=10 per group). **(D)** Level of anti-Scl-70 antibodies in the serum of PBS-, HOCl- or BLM-treated mice (n=10 per group). **(E-J)** Whole blood neutrophils from HOCl- or BLM-SSc or PBS control mice were assayed by flow cytometry (HOCl model: n = 15 PBS and n =15 HOCl; BLM model: n= 15 PBS and n=15 BLM). **(E)** Representative histogram plot (top) and quantification (bottom) showing Mac-1 expression in neutrophils from PBS- or HOCl-treated mice. **(F)** Quantification of the Mac-1 expression in neutrophils from PBS- or BLM-treated mice. **(G)** Representative histogram plot (top) and quantification (bottom) showing L-selectin expression levels in neutrophils from PBS- or HOCl-treated mice. **(H)** Quantification of the L-selectin expression levels in neutrophils from PBS- or BLM-treated mice. **(I)** Representative histogram plot (left) and quantification (right) showing ROS levels in neutrophils from PBS- or HOCl-treated mice. **(J)** Quantification of the ROS levels in neutrophils from PBS- or BLM-treated mice. The data represent the mean ± SD for all experiments. HOCl, hypochlorous acid; BLM, bleomycin; ROS, reactive oxygen species; FMO, fluorescence minus one.

FIGURE 3. Neutrophils mediate fibrosis in mouse SSc.
(A) Representative skin sections isolated from HOCl-SSc mice treated with IgG or with 1A8, respectively (original magnification 4x; Masson Trichrome staining). **(B)** Dermal thickness was measured for each group (n=11 per group). **(C)** Representative lung sections isolated from

HOCl-SSc mice treated with IgG or 1A8 (original magnification 20x; Masson Trichrome staining). **(D)** Microscopic scores of the lung sections according to a modified Ashcroft's method (right) were determined for HOCl mice treated with IgG or 1A8 (n=12 IgG and n= 13 HOCl). **(E)** Representative skin sections isolated from BLM-SSc mice treated with IgG or with 1A8, respectively (original magnification 4x; Masson Trichrome staining). **(F)** Dermal thickness was measured for each group (n=13 per group). **(G)** Representative lung sections isolated from BLM-SSc mice treated with IgG or with 1A8, respectively (original magnification 20x; Masson Trichrome staining). **(H)** Microscopic scores of lung sections according to a modified Ashcroft's method (right) were determined for BLM-SSc mice treated with IgG or 1A8 (n=13 IgG and n=12 BLM). **(I)** Representative skin sections isolated from WT mice 2 weeks following adoptive transfer (i.d injectction) of neutrophils isolated from PBS-, HOCl- or BLM-treated mice (original magnification 4x; Masson Trichrome staining). **(J-K)** Dermal thickness was measured for each group (HOCl model: n = 6 PBS and n = 6 HOCl; BLM model: n= 10 PBS and n=10 BLM). **(L)** Representative lung sections isolated from wild-type mice 2 weeks following adoptive transfer (i.v. injection) of neutrophils isolated from PBS-, HOCl- or BLM-treated mice (original magnification 20x; Masson Trichrome staining). **(M-N)** Microscopic scores of the lung sections according to a modified Ashcroft's method were determined for each group (HOCl model: n = 6 PBS and n = 6 HOCl; BLM model: n= 10 PBS and n=10 BLM). The data represent the mean ± SD.

FIGURE 4. NETs released by neutrophils participate in fibrosis in SSc.
(A) NET generation by human neutrophils was assayed *in vitro* after treatment with vehicle (DMSO) or A23187 (1μM) for 4h, assessing NET-bound CitH3 by ELISA (n= 7/group); each dot represents an independent experiment. **(B)** Levels of NET-bound CitH3 analyzed by ELISA from neutrophils isolated from wild-type mice treated with PBS (n=7) or HOCl (n=8) or from PAD4$^{-/-}$ (n=7) mice treated with HOCl. **(C)** Levels of NET-bound CitH3 analyzed by ELISA from neutrophils isolated from WT mice treated with PBS (n= 6) or BLM (n= 8) or from PAD4$^{-/-}$ (n=9) mice treated with BLM. **(D)** Levels of CitH3 in serum of PBS, HOCl or BLM mice analyzed by ELISA (n=10 per group). **(E)** Representative skin sections isolated from WT or PAD4$^{-/-}$ mice treated with HOCl, respectively (original magnification 4x; Masson Trichrome staining). **(F)** Dermal thickness was measured for each group (n=11 per group). **(G)** Representative lung sections isolated from WT or PAD4$^{-/-}$ mice treated with HOCl (original magnification 20x; Masson Trichrome staining). **(H)** Microscopic scores of lung sections according to a modified Ashcroft's method (right) were determined for each group (n=11 per group). **(I)** Representative skin sections isolated from PAD4$^{-/-}$ mice 2 weeks following adoptive transfer of neutrophils isolated from PBS- or HOCl-treated mice (original magnification 4x; Masson Trichrome staining). **(J)** Dermal thickness was measured for each group (n=8 per group). **(K)** Representative lung sections isolated from PAD4$^{-/-}$ mice 2 weeks following adoptive transfer of neutrophils isolated from PBS- or HOCl-treated mice (original magnification 20x; Masson Trichrome staining). **(L)** Microscopic scores of the lung sections according to a modified Ashcroft's method were determined for each group (n=8 per group). The data represent the mean ± SD. CitH3, citrullinated H3; NETs, neutrophil extracellular traps; PAD4, Peptidylarginine deiminase 4; WT, wild type.

FIGURE 5. Platelets are activated during SSc and participate in fibrosis.
(A-F) Whole blood platelets from dSSc patients and healthy controls (n=10 per group) and HOCl-SSc or BLM-SSc or PBS control mice (n=14 per group) were assayed by flow cytometry. **(A-C)** Quantification of the P-selectin expression levels on platelets from human dSSc patients **(A)**, mouse HOCl-SSc **(B)** or mouse BLM-SSc **(C)**, compared to healthy controls for each group. **(D-F)** Quantification of phosphatidyl serine expression on platelet surface from human dSSc patients **(D)**, mouse HOCl-SSc **(E)** or mouse BLM-SSc **(F)**, compared to healthy controls for

each group. **(G)** Representative skin sections isolated from Pf4^{cre-}-iDTR$^{fl/fl}$ (+ Platelets) or Pf4^{cre+}-iDTR$^{fl/fl}$ (- Platelets) mice treated with HOCl (original magnification 4x; Masson Trichrome staining). **(H)** Dermal thickness was measured for each group (n=8 per group). **(I)** Representative lung sections isolated from Pf4^{cre-}-iDTR$^{fl/fl}$ (+ Platelets) or Pf4^{cre+}-iDTR$^{fl/fl}$ (- Platelets) mice treated with HOCl (original magnification 20x; Masson Trichrome staining). **(J)** Microscopic scores of lung sections according to a modified Ashcroft's method (right) were determined for each group (n=8 per group). **(K)** Representative skin sections isolated from WT mice 2 weeks following adoptive transfer of platelets isolated from PBS- or HOCl-treated mice (original magnification 4x; Masson Trichrome staining). **(L)** Dermal thickness (was measured for each group (n=6 per group). **(M)** Representative lung isolated from WT mice 2 weeks following adoptive transfer of platelets isolated from PBS- or HOCl-treated mice (original magnification 20x; Masson Trichrome staining). **(N)** Microscopic scores of lung sections according to a modified Ashcroft's method (right) were determined for each group (n=6 per group). The data represent the mean ± SD.

FIGURE 6. Platelets trigger the profibrotic function of neutrophils in SSc.
(A-G) Whole blood platelet and neutrophil activation were assayed by flow cytometry (n= 15 per group). Kinetics of activation was assessed every 14 days in PBS and HOCl-SSc mice and platelet activation was monitored via change in P-selectin **(A)** and phosphatidyl serine **(B)** expression while neutrophil activation was monitored via change in the expression of Mac-1 **(C)** and L-selectin **(D)** and in ROS generation **(E)**. Mac-1 **(F)** and L-selectin **(G)** expression were assessed on neutrophils from Pf4^{cre-}-iDTR$^{fl/fl}$ (+ Platelets) or Pf4^{cre+}-iDTR$^{fl/fl}$ (- Platelets) mice treated with HOCl (n=6 per group). **(H)** Levels of NET-bound CitH3 analyzed by ELISA from WT neutrophils co-cultured for 4h with platelets isolated from PBS-, HOCl- or BLM-treated mice. Vehicle (DMSO) or A23187 (1µM) serve as control (n=5 per group). **(I)** Levels of NET-bound CitH3 analyzed by ELISA from healthy naive neutrophils co-cultured for 3h with platelets isolated from healthy control or dSSc patients. Vehicle (untreated) serves as control (n=4 per group). **(J)** Representative skin sections isolated from WT mice 2 weeks following adoptive transfer of neutrophils pre-incubated with platelets isolated from PBS or HOCl-treated mice (original magnification 4x; Masson Trichrome staining). **(K)** Dermal thickness was measured for each group (n=6 per group). **(L)** Representative lung sections isolated from WT mice 2 weeks following adoptive transfer of neutrophils pre-incubated with platelets isolated from PBS- or HOCl-treated mice (original magnification 20x; Masson Trichrome staining). **(M)** Microscopic scores of lung sections according to a modified Ashcroft's method (right) were determined for each group (n=6 per group). The data represent the mean ± SD. Plt, platelet.

FIGURE 7. The platelet-neutrophil axis of fibrosis in SSc is activated via the GPVI receptor.
(A-H) Whole blood platelets and neutrophils were assayed by flow cytometry in GPVI$^{-/-}$ or littermate control GPVI$^{+/+}$ mice treated with HOCl or BLM at d42 or d28, respectively (HOCl model: n = 13 PBS and n = 15 HOCl; BLM model: n= 15 PBS and n=14 BLM). Platelets were assayed for P-selectin and phosphatidyl serine expression in the HOCl **(A & C)** and the BLM **(B & D)** models. Neutrophils were assayed for Mac-1 and L-selectin expression in the HOCl **(E & G)** and the BLM **(F & H)** models. **(I)** Levels of CitH3 in serum of GPVI$^{-/-}$ or WT mice treated with HOCl analyzed by ELISA (n=10 per group). **(J)** Representative skin sections isolated from GPVI$^{+/+}$ or GPVI$^{-/-}$ mice treated with HOCl (original magnification 4x; Masson Trichrome staining). **(K)** Dermal thickness was measured for each group (n=12 PBS and n= 16 HOCl). **(L)** Representative lung sections isolated from GPVI$^{+/+}$ or GPVI$^{-/-}$ mice treated with HOCl (original magnification 20x; Masson Trichrome staining). **(M)** Microscopic scores of lung sections according to a modified Ashcroft's method (right) were determined for each group (n=12 PBS and n= 16 HOCl). **(N)** Representative skin sections isolated from GPVI$^{+/+}$ or GPVI$^{-/-}$ mice treated

with BLM (original magnification 4x; Masson Trichrome staining). **(O)** Dermal thickness was measured for each group (n=17 per group). **(P)** Representative lung sections isolated from $GPVI^{+/+}$ or $GPVI^{-/-}$ mice treated with BLM (original magnification 20x; Masson Trichrome staining). **(Q)** Microscopic scores of the lung sections according to a modified Ashcroft's method (right) were determined for each group (n=17 per group). The data represent the mean ± SD.

FIGURE 8. Platelets activate neutrophils to mediate fibrosis in scleroderma.
(1) Vascular injury exposes collagen, resulting in activation of circulating platelets via GPVI. (2) Platelets activate neutrophils, with effects including an increased propensity to release neutrophil extracellular traps (NETs). (3) Activated neutrophils and their NETs stimulate fibroblasts to produce fibrosis in skin and lung.

Figure 1: Neutrophils have a pro-inflammatory and pro-fibrotic phenotype in human dSSc

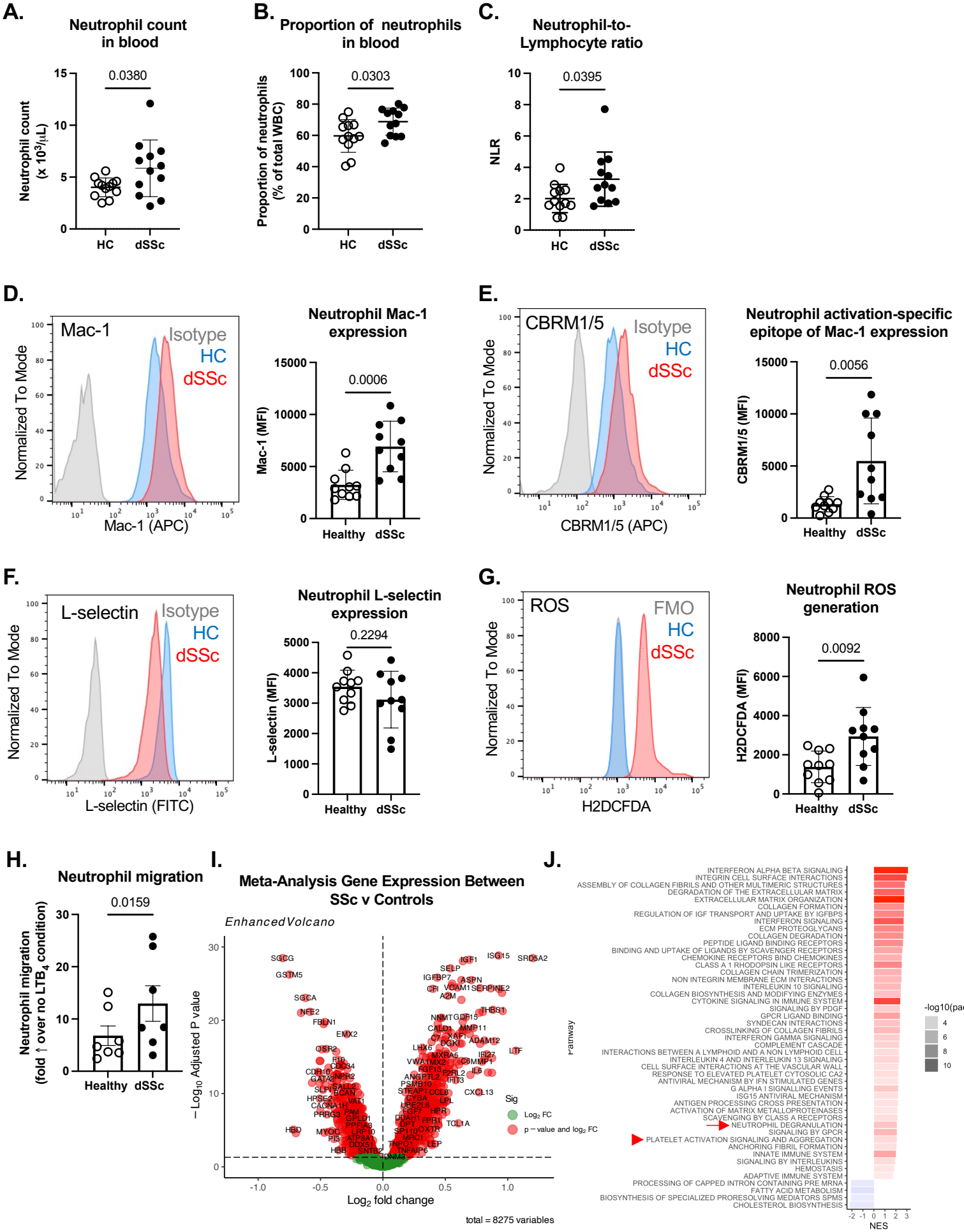

Figure 2: The HOCl and BLM models recapitulate aspects of the human phenotype of dSSc

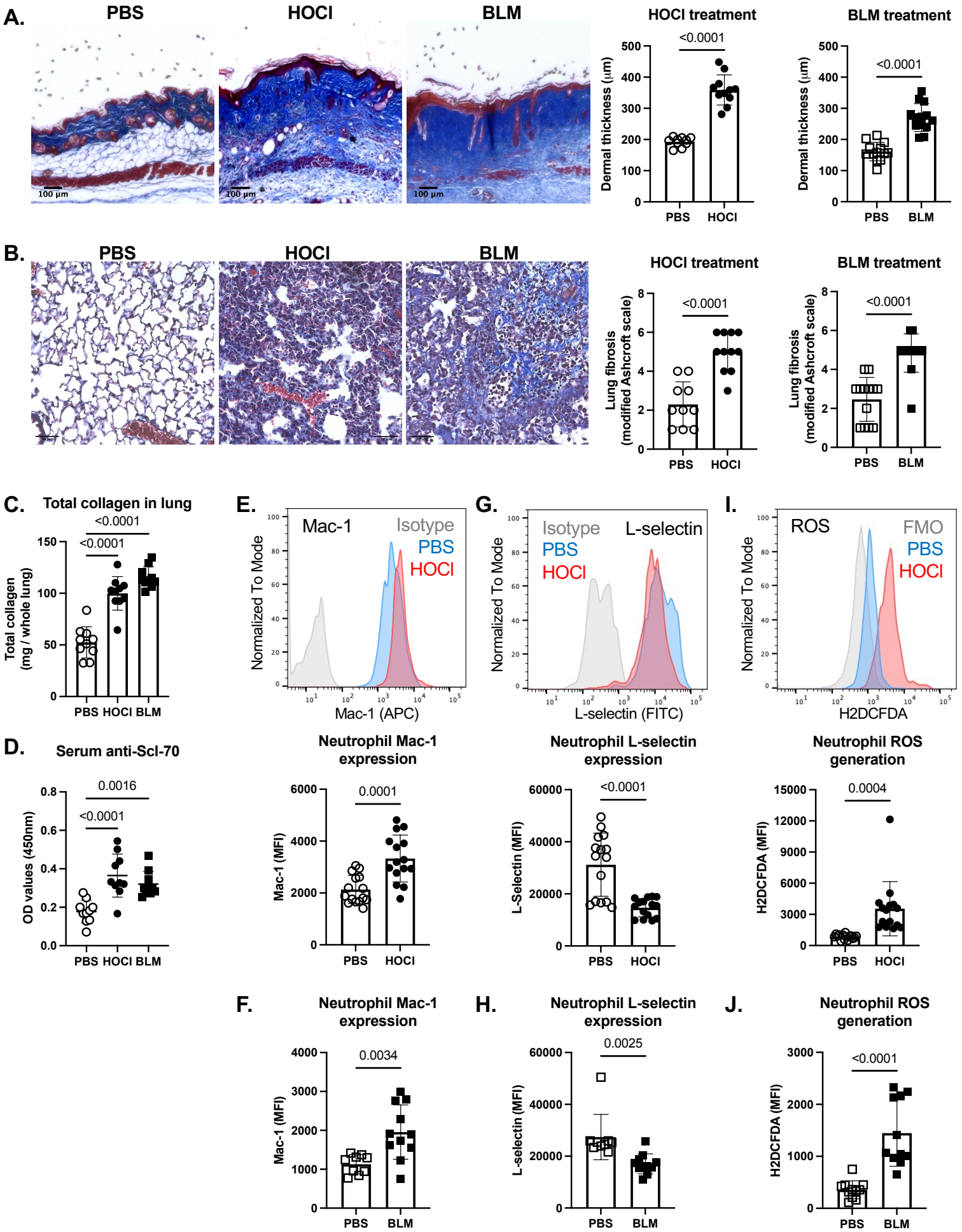

Figure 3: Neutrophils participate in fibrosis in mouse SSc

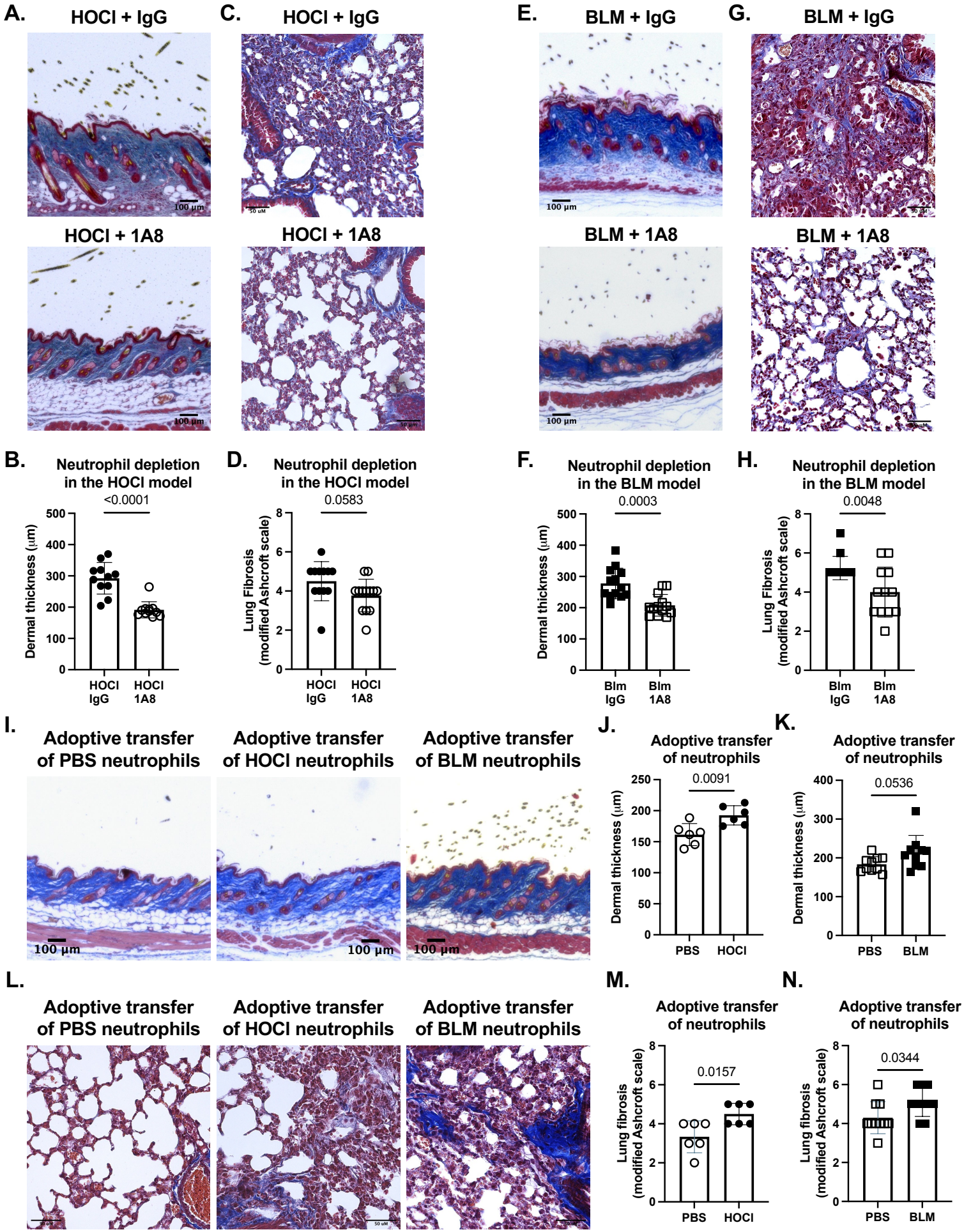

Figure 4: NET release is increased in SSc neutrophils and participates in fibrosis

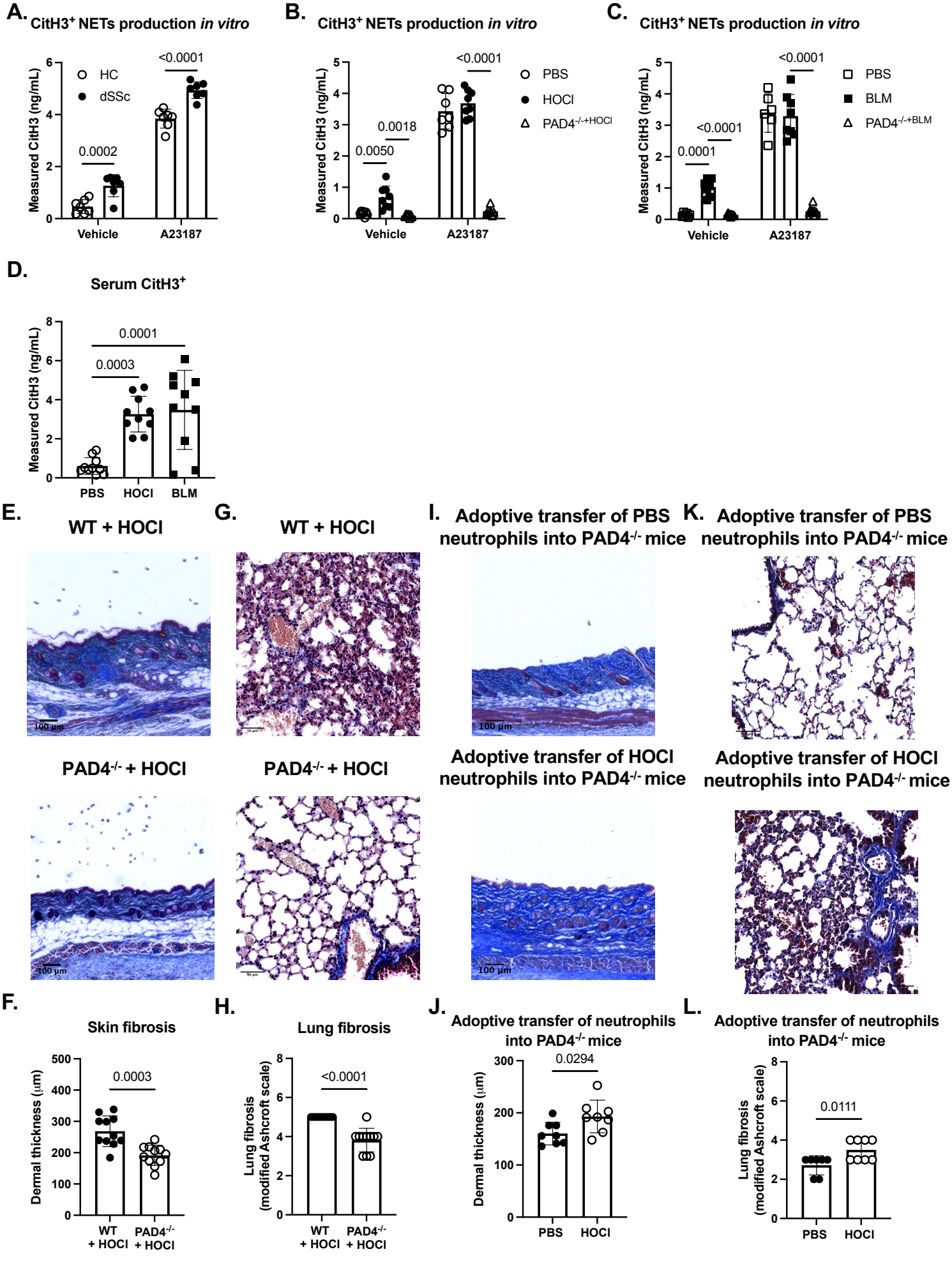

Figure 5: Platelets are activated during SSc and participate in fibrosis

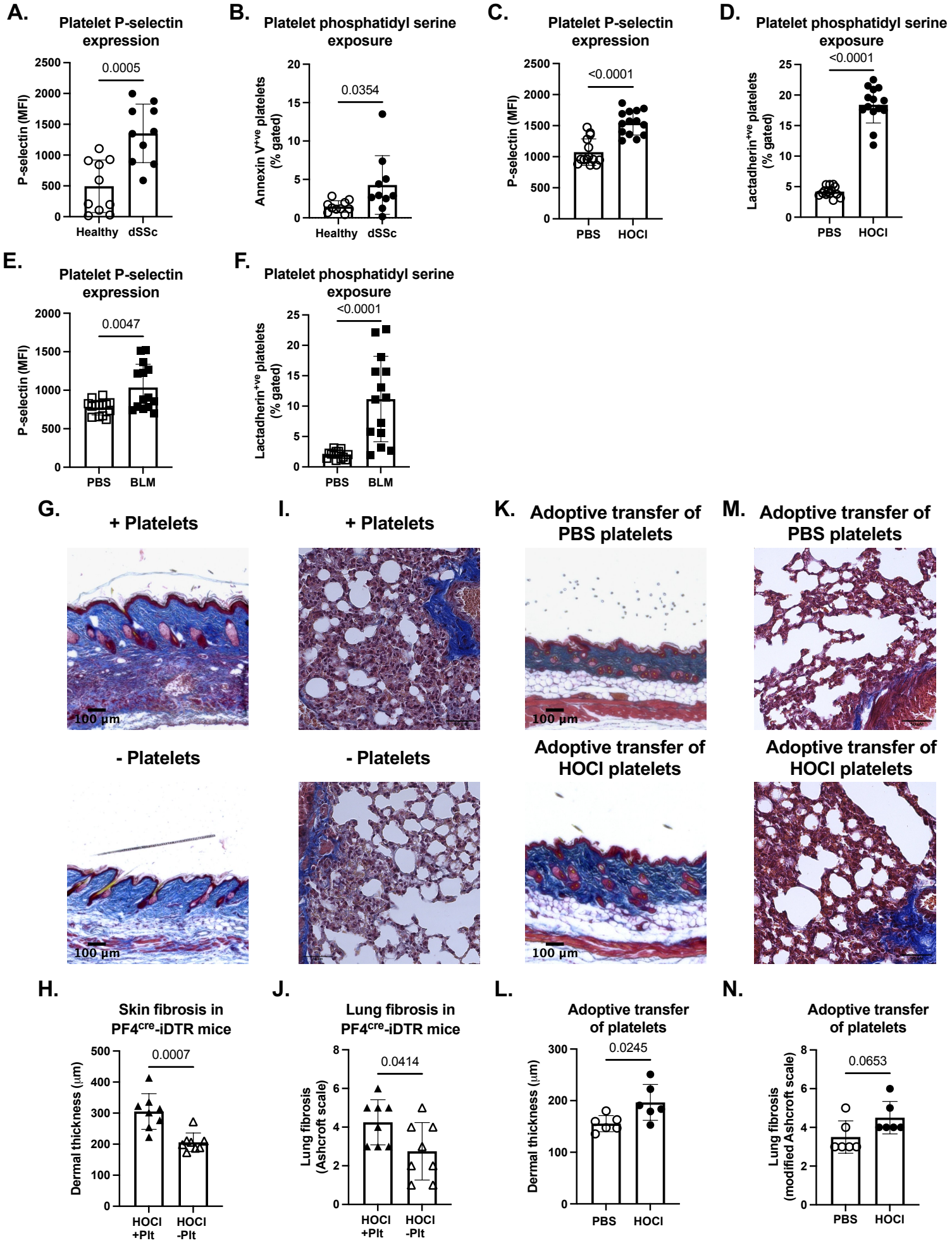

Figure 6: Platelets trigger the profibrotic function of neutrophils in SSc

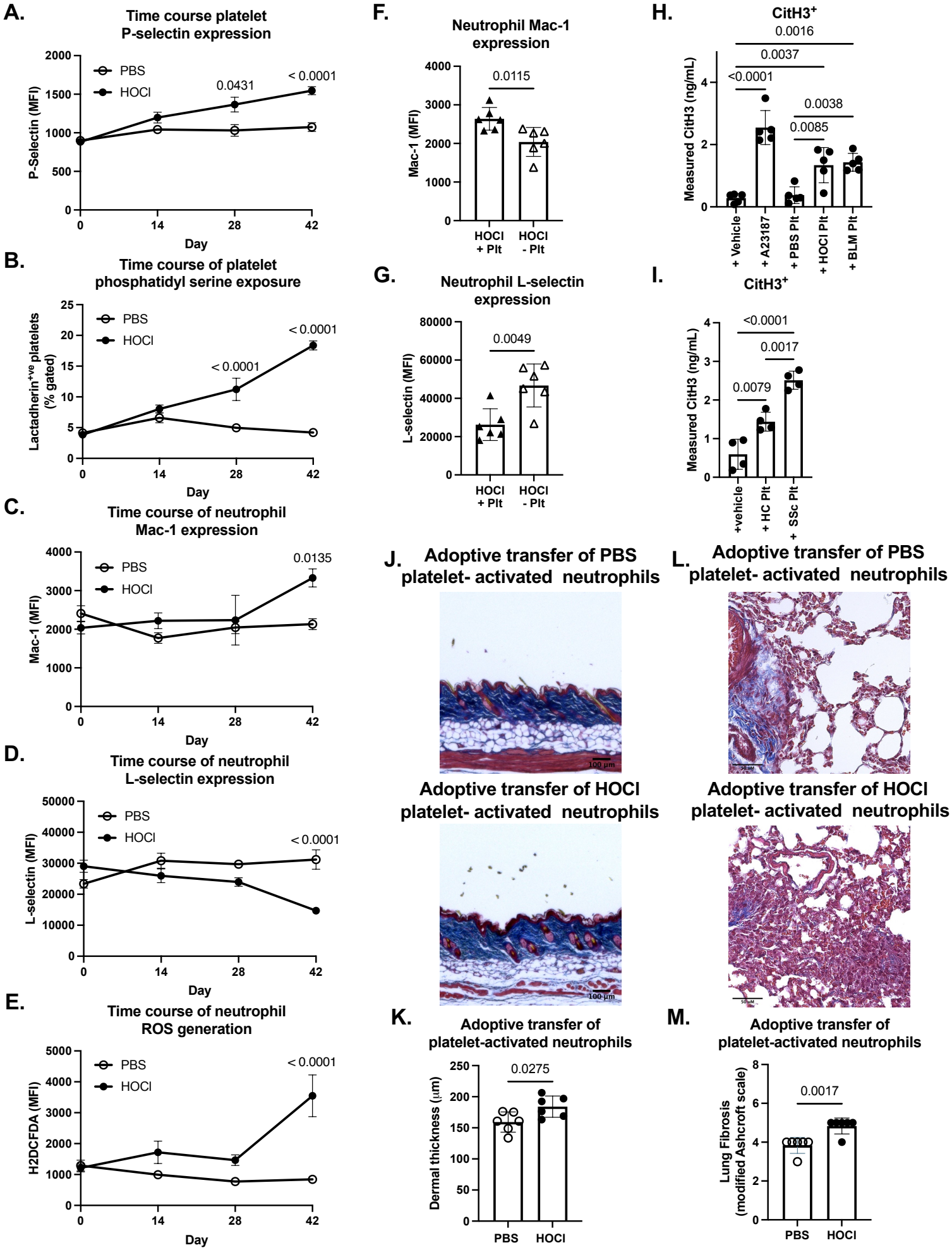

Figure 7: The platelet-neutrophil axis of fibrosis in SSc is mediated through the GPVI receptor

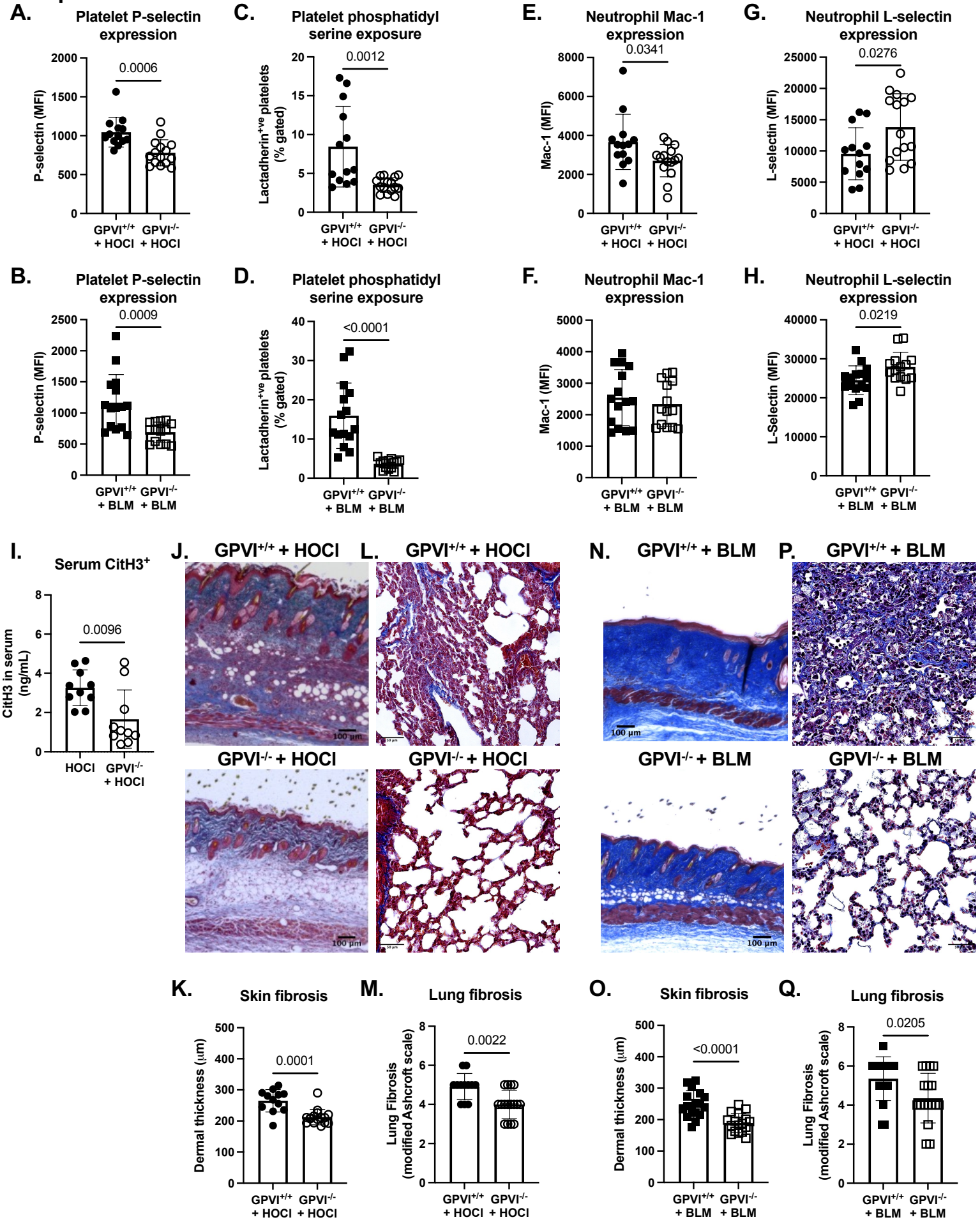
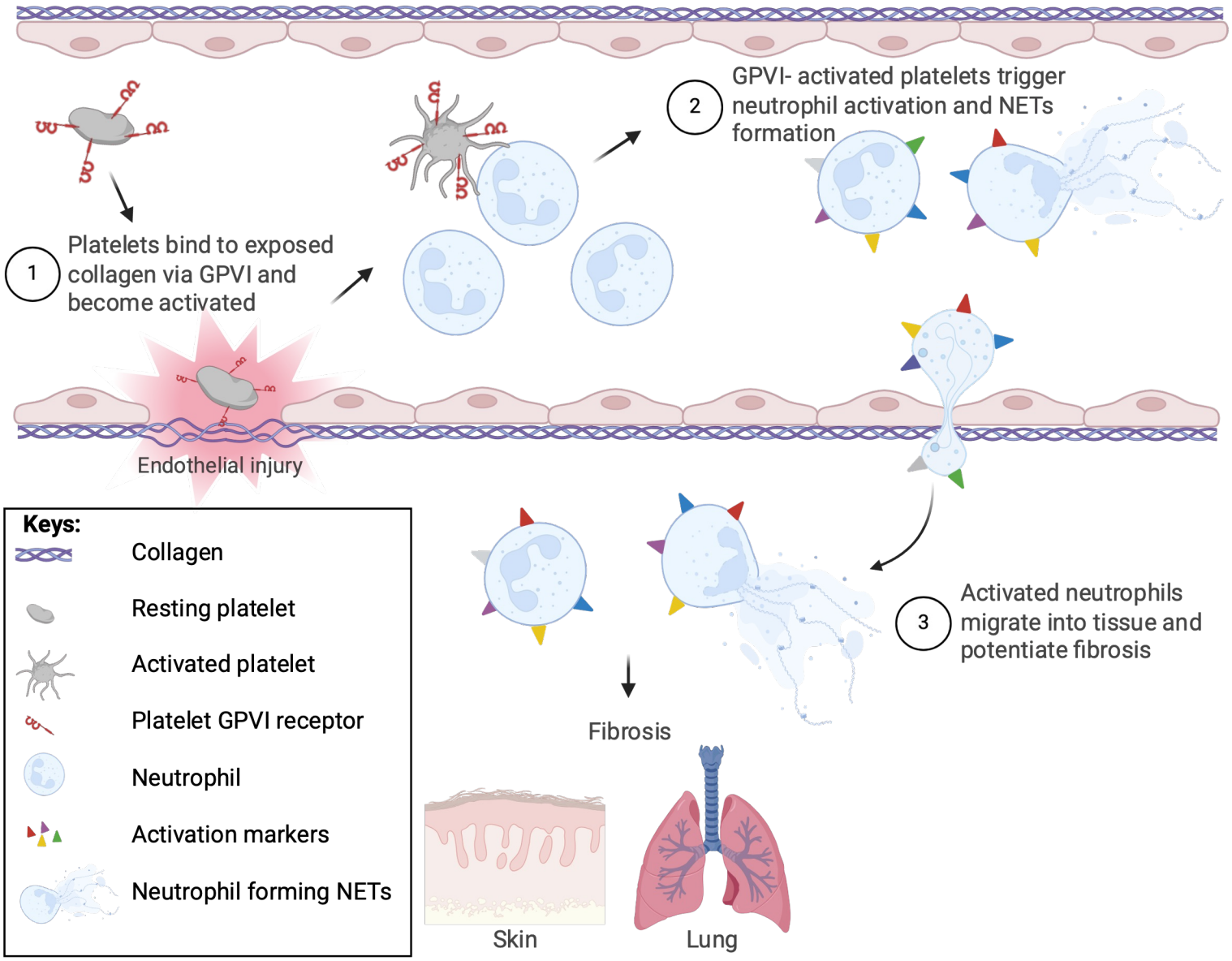
Figure 8: A GPVI-platelet-neutrophil-NET axis drives systemic sclerosis